AD-A074 892 UNITED TECHNOLOGIES RESEARCH CENTER EAST HARTFORD CONN F/G 20/5
INVESTIGATION OF PLASMA PROCESSES IN ELECTRONIC TRANSITION LASE--ETC(U)
SEP 79 W L NIGHAN N00014-76-C-0847
UNCLASSIFIED UTRC/R79-922617-4 NL

| OF |
AD
A074892

END
DATE FILMED
11-79
DDC

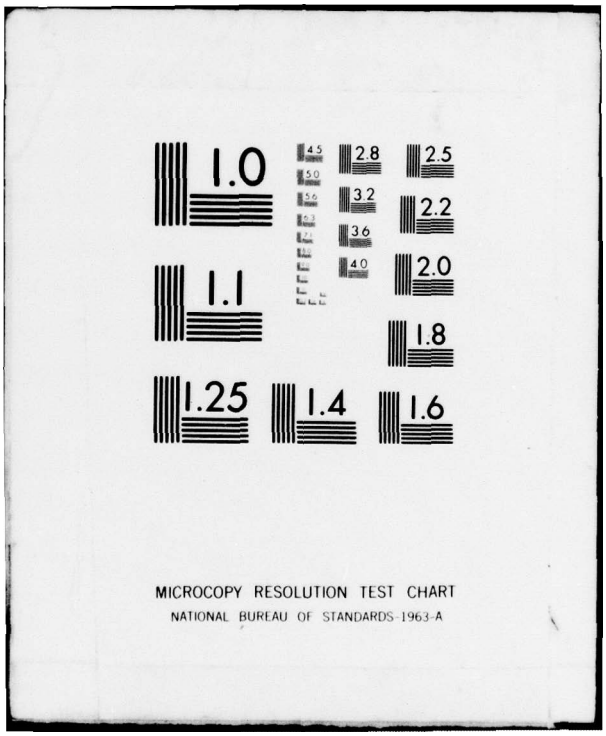
1.0
1.1
1.25
1.4
1.6
1.8
2.0
2.2
2.5
2.8
3.2
3.6
4.0
4.5
5.0
5.6
MICROCOPY RESOLUTION TEST CHART
NATIONAL BUREAU OF STANDARDS-1963-A

(14) UTRC/R79-922617-4

LEVEL II (12)

(6) INVESTIGATION OF PLASMA PROCESSES IN ELECTRONIC TRANSITION LASERS'

Prepared by

(10) William L. Nighan

(9) Technical Report, 1 Jul 78 - 1 Jul 79

September 1, 1979

(11) 1 Sep '79 (12) 36

Sponsored by the Office of Naval Research

Under Contract (15) N00014-76-C-0847

UNITED TECHNOLOGIES RESEARCH CENTER

EAST HARTFORD, CONNECTICUT 06108

77-08-221-1

Report R79-922617-4

INVESTIGATION OF PLASMA PROCESSES IN ELECTRONIC TRANSITION LASERS

William L. Nighan

Technical Report
September 1, 1979

Sponsored by the Office of Naval Research
under Contract N00014-76-C-0847

United Technologies Research Center
East Hartford, Connecticut 06108

SECURITY CLASSIFICATION OF THIS PAGE (When Data Entered)

REPORT DOCUMENTATION PAGE

READ INSTRUCTIONS BEFORE COMPLETING FORM

1. REPORT NUMBER: R79-922617-4
2. GOVT ACCESSION NO.:
3. RECIPIENT'S CATALOG NUMBER:

4. TITLE (and Subtitle): Investigation of Plasma Processes in Electronic Transition Lasers
5. TYPE OF REPORT & PERIOD COVERED: Technical Report, July 1, 1978 - July 1,1979
6. PERFORMING ORG. REPORT NUMBER: R79-922617-4

7. AUTHOR(s): William L. Nighan
8. CONTRACT OR GRANT NUMBER(s): N00014-76-C-0847

9. PERFORMING ORGANIZATION NAME AND ADDRESS: United Technologies Research Center, Silver Lane, East Hartford, CT. 06108
10. PROGRAM ELEMENT, PROJECT, TASK AREA & WORK UNIT NUMBERS:

11. CONTROLLING OFFICE NAME AND ADDRESS: Office of Naval Research, Physics Program Office, 800 N. Quincy Street, Arlington, VA. 22717
12. REPORT DATE: September 1, 1979
13. NUMBER OF PAGES: 37

14. MONITORING AGENCY NAME & ADDRESS(if different from Controlling Office):
15. SECURITY CLASS. (of this report): Unclassified
15a. DECLASSIFICATION/DOWNGRADING SCHEDULE:

16. DISTRIBUTION STATEMENT (of this Report)
Approved for public release; distribution unlimited. Reproduction in whole or in part is permitted for any purpose of the United States Government.

17. DISTRIBUTION STATEMENT (of the abstract entered in Block 20, if different from Report)

18. SUPPLEMENTARY NOTES
To be published in Applied Physics Letters

19. KEY WORDS (Continue on reverse side if necessary and identify by block number)
Mercury-halide lasers, mercuric-bromide dissociation laser, plasma processes in $HgBr_2$ laser discharges, $N_2^*(A)$-$HgBr_2$ excitation transfer, $N_2^*(B)$-$HgBr_2$ excitation transfer.

20. ABSTRACT (Continue on reverse side if necessary and identify by block number)
This paper reports the results of an analysis of basic kinetic and plasma processes in fast-pulse (~ 100 nsec) electric discharges containing mixtures of the mercuric-bromide molecule $HgBr_2$, and N_2 in a Ne background. Formation of the laser molecule HgBr ($B^2\Sigma^+$) is shown to occur as result of dissociative excitation transfer following quenching of N_2 ($A^3\Sigma_u^+$) by $HgBr_2$.

DD FORM 1 JAN 73 1473 EDITION OF 1 NOV 65 IS OBSOLETE
S/N 0102-LF-014-6601

Unclassified
SECURITY CLASSIFICATION OF THIS PAGE (When Data Entered)

PREFACE

Under the present ONR Contract, United Technologies Research Center is conducting an analytical investigation of plasma processes in electrically excited electronic transition lasers. Particular emphasis in this investigation is directed toward analysis of mercury-halide lasers, XeCl lasers using HCl as the halogen source, and advanced heavy-metal systems such as TlHg. A primary objective of this research is identification of fundamental mechanisms influencing laser and plasma processes. This work is being carried out in close coordination with other Corporate and Navy sponsored experimental and theoretical programs.

The present technical report is based upon a paper entitled "Kinetic Processes in the Electrically Excited Mercuric-Bromide Dissociation Laser" which has been submitted to Applied Physics Letters. Reprints of recently published papers are also included in an appendix.

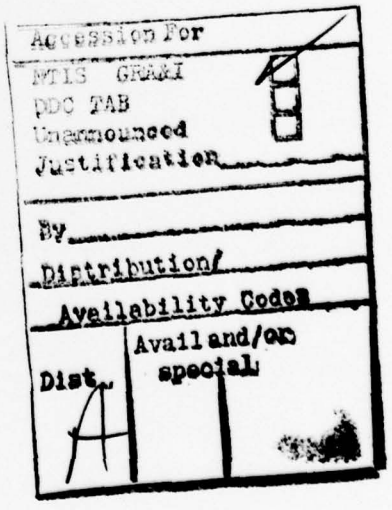

Investigation of Plasma Processes in
Electronic Transition Lasers

TABLE OF CONTENTS

Kinetic Processes in the Electrically Excited Mercuric-Bromide Dissociation Laser*

by

William L. Nighan

United Technologies Research Center

East Hartford, Connecticut 06108

Abstract

This paper reports the results of an analysis of basic kinetic and plasma processes in fast-pulse ($\sim$ 100 nsec) electric discharges containing mixtures of the mercuric-bromide molecule $HgBr_2$, and N_2 in a Ne background. Formation of the laser molecule HgBr ($B^2\Sigma^+$) is shown to occur as result of dissociative excitation transfer following quenching of N_2 ($A^3\Sigma_u^+$) by $HgBr_2$.

* Supported in part by the Office of Naval Research

Excitation of the mercury-bromide $B^2\Sigma^+ \rightarrow X^2\Sigma^+$ laser transition at 502 nm has been achieved by dissociative excitation of the mercuric-bromide molecule, $HgBr_2$, in an electric discharge[1,2]. Electrical-optical energy conversion efficiency in the 0.1 - 1.0% range has been obtained, suggesting that for optimized conditions efficiency in excess of 1% may be achievable. Moreover, the required concentration of $HgBr_2$ ($\sim$ 2 torr) can be produced at a temperature ($\sim$ 150°C) substantially lower than that typical of mercury-halide lasers using mercury vapor-halogen mixtures. In this paper basic kinetic processes occurring in this new class of mercury-halide laser will be examined.

Experimentation[1,2] using fast-pulse ($\sim$ 100 nsec) electric discharge excitation indicates an optimum $HgBr_2$ fractional concentraion in the 0.2 - 0.3% range with Ne (or He) serving as the buffer gas at a pressure near one atmosphere. Addition of approximately 2 - 10% N_2 to this mixture has been found to improve laser power and efficiency significantly. For this reason analysis of $HgBr(B^2\Sigma^+)$ formation kinetics in the N_2 laser mixture has been emphasized in the present study. Electron-N_2 collision processes are expected to dominate discharge processes in the $HgBr_2$ - N_2 - Ne mixture because of the large N_2:$HgBr_2$ concentration ratio, the numerous N_2 vibrational and electronic levels having large cross sections, and the high energy threshold for electronic excitation of Ne. Indeed, the present calculations of electron energy distributions and electron-molecule energy transfer rates for the E/n range typical of the experiments of Refs. 1 and 2 show that over 95% of the total discharge energy is consumed by N_2 vibrational and electronic excitation in approximately equal proportions. Recent measurements have shown that the rate

coefficient for dissociative excitation transfer from $N_2(A^3\Sigma_u^+)$ to $HgBr_2$ is large[3], and that the cross section for direct electron dissociative excitation of $HgBr_2$ leading to $HgBr(B^2\Sigma^+)$ is small[4]. These findings are consistent with the $HgBr(B^2\Sigma^+)$ formation sequence illustrated in Fig. 1.

Figure 1 shows the principal N_2 states excited directly by electron impact on ground state N_2. The shaded area refers to the $N_2(B'^3\Sigma_u^-)$, $(a'^1\Sigma_u^-)$, $(a^1\Pi_g)$ and $(w^1\Delta_u)$ group of states; and the percentages shown refer to the fractional electron energy initially transferred to each state (or group of states), computed for the experimental conditions of present interest[1,2]. There are numerous $HgBr_2$ electronic states in the 4-10 eV range.[5] In this figure, the regions labeled a-d refer to the experimentally determined photo-absorption bands of $HgBr_2$[1,5]. Available evidence indicates that only states in the "b" band, and particularly $HgBr_2(^3\Sigma_u^+)$ and $(^1\Sigma_u^+)$, predissociate to form $HgBr(B^2\Sigma^+)$.

Measurements[3] of $N_2(A^3\Sigma_u^+)$ quenching by $HgBr_2$ yield a rate coefficient of 1.0×10^{-10} sec^{-1}cm^3 for the formation of $HgBr(B^2\Sigma_u^+)$, and a total quenching coefficient of approximately 3.0×10^{-10} sec^{-1}cm^3, indicative of a branching ratio of about one-third. However, Fig. 1 shows that only 10% of the electron energy is transferred directly to $N_2(A^3\Sigma_u^+)$. Thus, a primary consideration in analysis of $HgBr(B^2\Sigma^+)$ formation kinetics in the $HgBr_2/N_2$ system is the ultimate redistribution of the large fraction ($\sim$ 40%) of the discharge energy initially deposited in higher N_2 electronic levels, particulary the coupled $B^3\Pi_g$ and $W^3\Delta_u$ states which are populated by electron impact and by cascade from higher levels. Under laser discharge conditions, excitation transfer from these states to $HgBr_2$ is likely to occur in

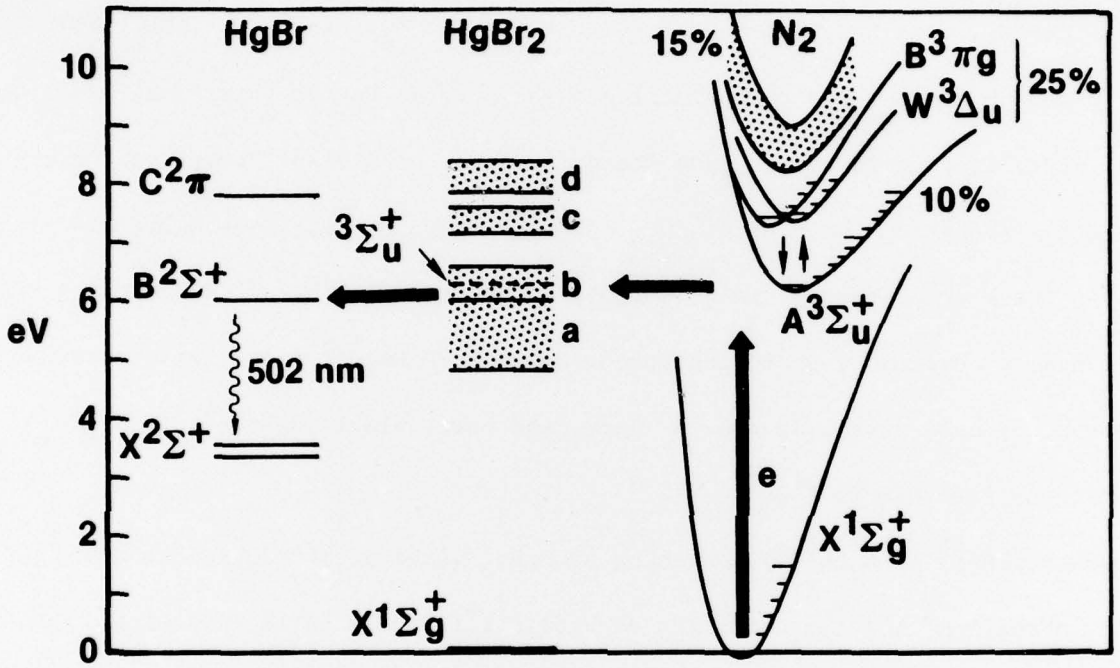

Fig. 1. Simplified energy level diagram illustrating the HgBr($B^2\Sigma^+$) formation sequence in electrically excited mixtures of $HgBr_2$ and N_2. The percentages shown refer to the fractional electron energy transfer to each state.

a time less that that required for either electronic relaxation to high vibrational levels of $N_2(A^3\Sigma_u^+)$, or for vibrational relaxation of the $A^3\Sigma_u^+$ state. Michels[6] has carried out an analysis based on consideration of the energy defect corresponding to various N_2^* - $HgBr_2$ collision channels and on correlations of the spin and symmetry of reaction products. This analysis shows that excitation transfer from $N_2(A^3\Sigma_u^+)$ results in the formation of $HgBr_2(^3\Sigma_u^+)$ which correlates diabatically with the $HgBr(B^2\Sigma^+)$ laser state, with some branching to $HgBr(A^2\Pi)$ and $HgBr(X^2\Sigma^+)$ also probable. This conclusion is consistent with measurements[3] of $N_2(A^3\Sigma_u^+)$ quenching by $HgBr_2$. In contrast to this situation, excitation transfer from $N_2(W^3\Delta_u)$ leads to $HgBr_2(^3\Delta_u)$, and subsequently to $HgBr(A^2\Pi)$ and $HgBr(C^2\Pi)$, with no branching to $HgBr(B^2\Sigma_u^+)$. In addition, excitation transfer from $N_2(B^3\Pi_g)$ leads to $HgBr_2(^3\Pi_g)$, which correlates diabatically with the $HgBr(C^2\Pi)$ state, with branching to the $A^2\Pi$, $B^2\Sigma^+$ and $X^2\Sigma^+$ states of HgBr also possible. Thus, excitation transfer to $HgBr_2$ from the coupled $B^3\Pi_g$ and $W^3\Delta_u$ states of N_2 is expected to result in states of $HgBr_2$ which, for the most part, do not dissociate to produce the $HgBr(B^2\Sigma^+)$ laser state. In the present analysis, the total rate coefficient for quenching of $N_2(B^3\Pi_g)$ and $N_2(W^3\Delta_u)$ was taken to be the same as the value measured for $N_2(A^3\Sigma_u^+)$, but branching to $HgBr(B^2\Sigma^+)$ was assumed to be zero.

Because N_2 cross sections for vibrational and electronic excitation are well known, electron energy distributions and related rate coefficients could be calculated reliably for use as input in a self-consistent model of the time dependent variation of electron, ion and excited state processes for conditions typical of

the fast-pulse discharge experiments of Refs. 1 and 2. For a $Ne-N_2-HgBr_2$ mixture in the proportions 0.95 - 0.05 - 0.0025 at a pressure of 1.3 atm, the measured[1] E/n value at which breakdown occurred was found to be approximately $3 \times 10^{-16} Vcm^2$, subsequently decreasing to zero in about 150 nsec. For these conditions the present calculations show that the dominant contributions to ionization are Penning ionization of N_2 and $HgBr_2$ by Ne* ($\sim$ 50%), direct electron impact ionization of N_2 ($\sim$ 35%), and direct electron impact ionization of $HgBr_2$ ($\sim$ 15%)[7]. Ionization from the highly populated $N_2(A^3\Sigma_u^+)$, $(B^3\Pi_g)$ and $(W^3\Delta_u)$ states was found to be unimportant, a reflection of the relatively high ionization potentials of these excited species. This is significant, since cumulative ionization involving electronically excited species is usually a major contributor to the occurrence of ionization instability and subsequently, discharge arcing[8].

Presented in Fig. 2 are temporal variations of discharge current density, zero-field gain (assuming no lower laser level population), and the energy efficiency of $HgBr(B^2\Sigma^+)$ formation computed for conditions typical of those of Ref. 1. The $HgBr(B^2\Sigma^+)$ formation efficiency at any point is simply the time integrated ratio of the energy flow through the $HgBr(B^2\Sigma_u^+)$ state to the total energy deposited in the discharge up to that time. Both the peak values and temporal evolution of the computed current density and gain are in good agreement with measured values[1]. For the conditions of this example $HgBr(B^2\Sigma^+)$ is produced by way of excitation transfer from the $N_2(A^3\Sigma_u)$ state alone as discussed previously, the latter produced by direct electron impact of N_2, and to a lesser extent by $N_2(B^3\Pi_g) \rightarrow N_2(A^3\Sigma_u^+)$ transitions resulting from collisions with electrons and N_2 molecules. The primary loss of

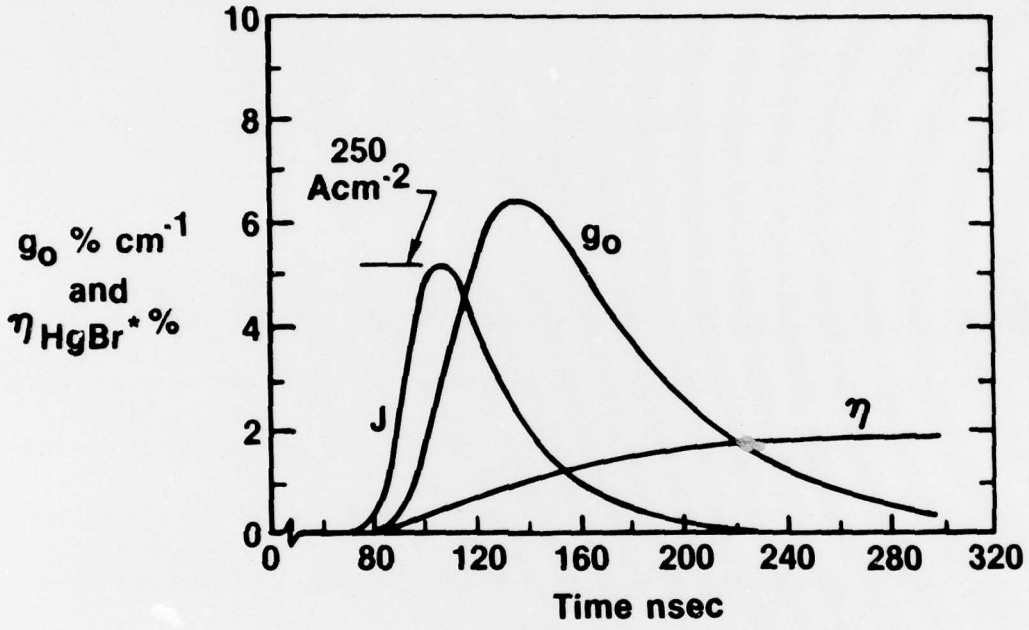

Fig. 2. Temporal variations of discharge current density, zero-field gain (assuming no lower laser level population), and $HgBr(B^2\Sigma^+)$ formation efficiency computed for a $Ne-N_2-HgBr_2$ mixture in the proportions 0.95-0.05-0.0025 at a pressure of 1.3 atm and conditions otherwise similar to the experiments of Ref. 1.

$HgBr(B^2\Sigma^+)$ is due to spontaneous decay ($\sim$ 47%), and to collisions with $HgBr_2$ ($\sim$ 17%), Ne ($\sim$ 16%), electrons ($\sim$ 13%) and N_2 ($\sim$ 7%). These processes result in an effective upper level lifetime of about 10 nsec, corresponding to a saturation intensity of approximately 175 kW/cm^2; also in good agreement with measured values[1]. Figure 2 indicates that $HgBr(B^2\Sigma^+)$ formation efficiency reaches a maximum level of about 2.0% by the end of the pulse. Measured[1] laser efficiency under these conditions is typically 0.5%, a value consistent with an overall optical extraction efficiency of 25%.

Figure 3 shows the temporal variation of several major species corresponding to the conditions of Fig. 2. The concentrations of the $N_2(A^3\Sigma_u^+)$ and the coupled $N_2(B^3\Pi_g)$ and $N_2(W^3\Delta_u)$ states reach very high levels at about the time the current density reaches its peak, reflecting the relatively large values of N_2 concentration, electron density, and e-N_2 excitation rate coefficients. These N_2 states decay rather slowly indicative of their rate of quenching by $HgBr_2$ which is present in small concentration. In the present model the temporal decay of $HgBr(B^2\Sigma^+)$ essentially follows the $N_2(A^3\Sigma_u^+)$ population as shown in the figure. However, vibrational redistribution within the $N_2(A^3\Sigma_u^+)$ state will occur as a function of time, particularly as the pumping decreases (decreasing n_e and E/n). Indeed, both the total $N_2(A^3\Sigma_u^+)$ quenching rate and $HgBr_2$ product states may actually exhibit a dependence on $N_2(A^3\Sigma_u^+)$ vibrational level, and therefore on time.

Fractional dissociation of $HgBr_2$ reaches a value of approximately 10% for the present example, resulting in a significant concentration of $HgBr(X^2\Sigma^+)$ by the end of the pulse. A significant fraction of $HgBr(X^2\Sigma^+)$ is initially produced in the v = 22 terminal laser level which is apparently relaxed rather rapidly by collisions

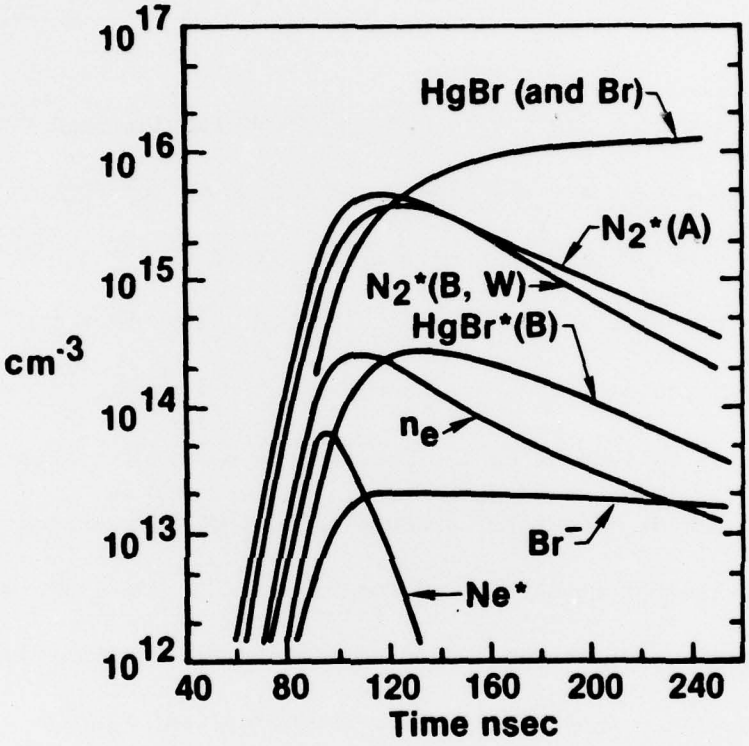

Fig. 3. Temporal variation of selected species concentrations corresponding to the conditions of Fig. 2.

with neutrals. However, since the electron density and electron temperature remain relatively high throughout the entire pulse, vibrational excitation of HgBr by electrons may result in a vibrational temperature well above that typical of the gas temperature. Thus, it is probable that lower laser level buildup becomes significant at some time prior to the end of the pulse for the conditions examined here.

Although addition of N_2 to the Ne-$HgBr_2$ mixture results in a significant improvement in pulse energy and efficiency, particularly the former, the $HgBr_2$ dissociation laser does operate at an efficiency above 0.1% without N_2 in the mixture[1]. The present analysis shows that electron energy transfer, ionization, and $HgBr(B^2\Sigma^+)$ formation processes are completely different in the absence of N_2. Calculations indicate that in Ne-$HgBr_2$ mixtures the dominant electron energy transfer processes are Ne metastable production followed by Penning ionization of $HgBr_2$, and direct electron impact ionization of $HgBr_2$[7]. Predissociating states of $HgBr_2$ can be produced either by the ion-ion recombination reaction, $HgBr_2^+ + B_r^- + Ne \rightarrow HgBr_2^* + Br + Ne$, or by electron-ion recombination, $HgBr_2^+ + e \rightarrow HgBr_2^*$. Based on estimates for ion loss rates[9], the present calculations show that ion loss due to electron-ion recombination is 5-10 times larger that that due to ion-ion recombination. Since numerous excited states of $HgBr_2$ can be formed by either recombination reaction, the branching ratio for $HgBr(B^2\Sigma^+)$ formation is not likely to be very high. By assuming a branching ratio of 0.2 for $HgBr(B^2\Sigma^+)$ formation via recombination reactions, values of peak gain ($\sim$ 4% cm^{-1}) and $HgBr(B^2\Sigma^+)$ formation efficiency ($\sim$ 1.75%) were computed for conditions generally similar to those of Fig. 2. These values are somewhat less than those typical of mixtures containing

N_2, a result consistent with experimental observations[1]. However, for similar current density levels the total energy deposited in the gas is significantly less in the absence of N_2 reflecting substantially lower E/n levels typical of Ne-$HgBr_2$ mixtures. It should also be pointed out that with N_2 in the mixture, recombination reactions are insignificant compared to $N_2(A^3\Sigma_u^+)$ excitation transfer insofar as $HgBr(B^2\Sigma^+)$ formation is concerned.

Although the data base required for comprehensive modeling of mercuric-bromide dissociation lasers is far from complete, the present analysis shows that available experimental observations can be interpreted in a self consistent manner for $HgBr_2$ laser mixtures containing N_2. Analysis of $HgBr(B^2\Sigma^+)$ formation kinetics and discharge characteristics indicate that the $HgBr_2/N_2$ system has considerable potential for efficient scaling to energy levels substantially in excess of those reported to date.

The author acknowledges numerous helpful discussions with his collegues particularly, L. A.Newman and H. H. Michels. Also, the expert assistance of L. Bromson with the numerical work is much appreciated. Additionally, the author thanks E. J. Schimitschek and R. Burnham for access to experimental data prior to publication.

REFERENCES

* Supported in part by the Office of Naval Research.

1. E. J. Schimitschek and J. E. Celto: Opt. Lett. 2, 64 (1978); also, Appl. Phys. Lett. (in press).

2. R. Burnham: Appl. Phys. Lett. 33, 156 (1978).

3. R. S. F. Chang and R. Burnham: Appl. Phys. Lett. (in press).

4. J. Allison and R. N. Zare: Chem. Phys. 35, 263, (1978).

5. K. Wieland: Z. Phys. 77, 157 (1932); also, W. R. Wadt: J. Chem. Phys., (in press).

6. H. H. Michels: Private communication.

7. For the purpose of the present analysis the ionization cross section for $HgBr_2$ has been assumed to increase from threshold at 10.6 eV to a peak value of 5×10^{-16} $V cm^2$ in the 50-100 eV range. The rate coefficient for dissociative attachment of $HgBr_2$ was taken as 1×10^{-10} sec^{-1} cm^3. The results presented in Figs. 2 and 3 were found to be relatively insensitive to variations in the $HgBr_2$ ionization and attachment rate coefficients.

8. R. T. Brown and W. L. Nighan: Appl. Phys. Lett. 32, 730 (1978).

9. In this analysis an effective electron-ion recombination coefficient of 1.0×10^{-7} sec^{-1} cm^3 was used for $HgBr_2^+$, along with a value of 3×10^{-7} sec^{-1} cm^3 for the reaction $HgBr_2^+ + Br^- + Ne \rightarrow HgBr_2^* + Br + Ne$, as recently computed by M. R. Flannery (private communication).

APPENDIX

REPRINTS OF RECENTLY PUBLISHED PAPERS

"Stability Enhancement in Electron-Beam Sustained Excimer Laser Discharges", R. T. Brown and W. L. Nighan. Applied Physics Letters, Vol. 35, pp. 142-144, 15 July 1979.

"Plasma Processes in Electron-Beam Controlled Rare-Gas Halide Lasers", W. L. Nighan, IEEE journal of Quantum Electronics, Vol. QE-19, pp. 714-726, October 1978 (invited paper).

Stability enhancement in electron-beam-sustained excimer laser discharges[a)]

Robert T. Brown and William L. Nighan
United Technologies Research Center, East Hartford, Connecticut 06108

(Received 9 April 1979; accepted for publication 4 May 1979)

Techniques are described for prolonging the duration of stable e-beam-controlled excimer laser discharges, including: temporal tailoring of either the discharge voltage or the ionization source and kinetics modification by way of additives. Theoretical and experimental results are presented for KrF^* laser discharges.

PACS numbers: 42.55.Hg, 52.35.Py, 52.80. – s

For practical high-power excimer laser systems, it is desirable to utilize electron-beam-sustained discharge excitation rather than electron-beam excitation alone, since for a given laser output power the burden on the electron-beam technology is significantly lower. One of the major obstacles to implementing the e-beam-sustained discharge technique is the onset of ionization instability.[1-3] In this paper a number of techniques for improving excimer laser discharge stability are outlined and theoretical and experimental results are presented for an electron-beam sustained KrF^* laser discharge.

It has been shown[2,3] that the major factor contributing to instability in electron-beam-controlled KrF^* laser discharges is dissociation of the molecular halogen, F_2, during the discharge pulse. This can be readily appreciated upon examination of the following approximate expression[1-3] for the instability growth rate ν, i.e.,

$$\nu \simeq 2n^* k_i^* - n_{F_2} k_a , \tag{1}$$

where n^* and n_{F_2} are the number densities of rare-gas metastable atoms and fluorine molecules, respectively, while k_i^* and k_a are the rate coefficients for metastable ionization and electron dissociative attachment, respectively. For conditions typical of KrF^* laser mixtures,[3] the electron conservation equation is well approximated by the relation

$$nS \simeq n_e n_{F_2} k_a , \tag{2}$$

and the metastable conservation equation can be approximated by

$$n_e n k_{ex}(E/n) \simeq n^* n_{F_2} k_Q , \tag{3}$$

where n is the density of ground-state rare-gas atoms, S is the ionization rate due to the electron beam, $k_{ex}(E/n)$ is the metastable production rate coefficient (exhibiting a very strong E/n dependence[3]), and k_Q is the rate coefficient for the loss of metastables due to F_2 quenching. Combination of Eqs. (1)–(3) yields the following criterion for discharge *sta-*

a)Supported in part by the Naval Ocean Systems Center and by the Office of Naval Research.

 0003-6951/79/020142-03$00.50

bility (i.e., $\nu < 0$):

$$\frac{2n^2 k_i^* S k_{ex}(E/n)}{n_{F_2}^3 k_a^2 k_Q} < 1 \tag{4}$$

For the parameter values required for efficient rare-gas–halide laser operation, it has been shown[3] that the left-hand side of this inequality is usually in the 0.1–0.5 range, indicative of a marginally stable situation.

In most e-beam-controlled KrF* lasers the discharge E/n value is typically maintained at a relatively constant level throughout the pulse, while the e-beam source function S tends to increase due to the space-charge-limited mode of operation of cold-cathode e-beam guns. This tendency results in an increase in the numerator on the left-hand side of inequality (4), i.e., reduced stability. More importantly, the form of Eq. (4) indicates that the onset of instability ($\nu > 0$) is exceptionally sensitive to the dissociative loss of F_2. Since F_2 dissociation is primarily a consequence of rare-gas–halide formation itself,[3] invariably a point in time is reached for which electron density disturbances are amplified, i.e., inequality (4) is violated and the discharge becomes unstable. At the high values of E/n (i.e., higher values of k_{ex}) required for effective discharge energy enhancement and high discharge power density, the unstable point is reached earlier in the pulse.[2,3]

The form of the stability criterion [Eq. (4)] discussed above suggests several techniques for increasing the stable duration of the discharge pulse while maintaining laser properties near their optimum values. These include: (1) temporal tailoring of either the discharge voltage (E/n), i.e., controlled temporal reduction of k_{ex}, or of the e-beam ionization source function S in order to compensate for F_2 loss; (2) modification of the halogen kinetics in such a way that loss of F_2 has a less severe effect on the occurrence of instability.

The stabilizing influence of judicious temporal reduction in either S or k_{ex} (i.e., E/n) in order to compensate for the changes in plasma properties caused by the dissociative loss of F_2 is conceptually straightforward. The potential role of halogen kinetics modification is best understood by observing that in conventional KrF* mixtures reactions involving F_2 control *both* the electron density [Eq. (2)] and the metastable density [Eq. (3)], a circumstance leading to the cubic dependence on F_2 concentration exhibited by inequality (4). This situation can be favorably altered by use of a two-component halogen mixture in which one species tends to dominate electron loss, while the other (the halogen fuel) dominates metastable processes and therefore excimer formation. Such is the case in certain F_2-NF_3 mixtures, for example. The rate coefficient for electron dissociative attachment in NF_3 is approximately four times *larger* than that of F_2, while the NF_3-rare-gas metastable atom quenching coefficient is about six times *smaller* than that of F_2. Thus, addition of a relatively small amount of NF_3 ($NF_3/F_2 < 0.1$) to the conventional KrF* laser mixture will significantly affect the electron density but should exert little or no influence on other processes. Enhanced stability should result as a consequence of the weakened coupling between the electron and metastable concentrations. Indeed,

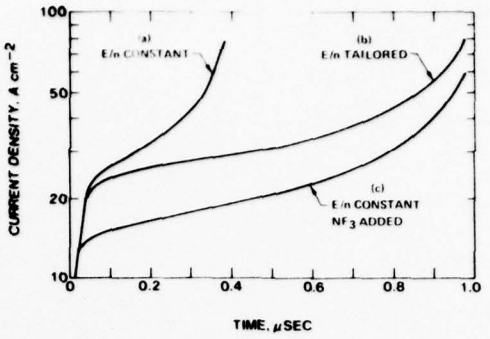

FIG. 1. Computed current density profiles for an e-beam-controlled Ar(0.95)-Kr(0.05)-F_2 (0.005) mixture at 1 atm. For each of these examples the *initial* E/n value was 1.4×10^{-16} V cm^2 and the e-beam ionization rate S was $150 + 7.5\times10^7 t$ sec^{-1}. (a) E/n constant; (b) E/n tailored according to the relation $1.4\times10^{-16} - 0.35\times10^{-10} t$ V cm^2; (c) E/n constant with 0.05% NF_3 added.

with NF_3 controlling the electron loss and F_2 the metastable loss, it is easily shown that the criterion for stability becomes

$$\frac{2n^2 k_i^* S k_{ex}(E/n)}{n_{F_2} k_Q (n_{NF_3} k_a)^2} < 1. \tag{5}$$

Since dissociative NF_3-metastable reactions will proceed at a much slower rate than the corresponding F_2 reactions, the impact of dissocation on electron density growth (plasma stability) should be lessened substantially as indicated by the linear dependence of Eq. (5) on F_2 concentration. Furthermore, use of NF_3 an acceptable fluorine donor itself, does not introduce processes unfavorable to the efficient formation of KrF*.

Detailed numerical evaluation of the stability enhancement techniques described above has been carried out using a comprehensive computer model of an e-beam-controlled KrF* laser discharge.[3] Representative results are presented in Fig. 1, which shows the characteristic temporal runaway of the discharge current density indicative of ionization instability onset [curve (a)].[1] For curve (a), E/n was maintained at a constant value of 1.4×10^{-16} V cm^2, a condition for which instability onset occurs approximately 0.3 μsec after discharge initiation. Curve (b) illustrates the effect of a controlled linear reduction in E/n from an initial value of 1.4×10^{-16} V cm^2 to a value of approximately 1.0×10^{-16} V cm^2 after 1.0 μsec. The predicted improvement in stability as reflected by the temporal variation in discharge current density is dramatic indeed, with the region of stable discharge behavior increasing to about 0.8 μsec, and the total energy deposited in the gas prior to the occurrence of instability increasing by almost a factor of 3. Moreover, the medium properties are sensibly uniform in time, having values compatible with efficient high-power laser operation,[4] e.g., KrF* production efficiency, 20%, zero-field gain, 2.5% cm^{-1}; gain : absorption ratio, 10; electric power density, 110 kW cm^{-3}; and time-integrated discharge energy enhancement, 5. Curve (c) illustrates the effect of NF_3 addition for an NF_3-F_2 concentration ratio of 0.1. The initially lower current density level reflects the increased attachment loss of electrons due the presence of NF_3. However, the im-

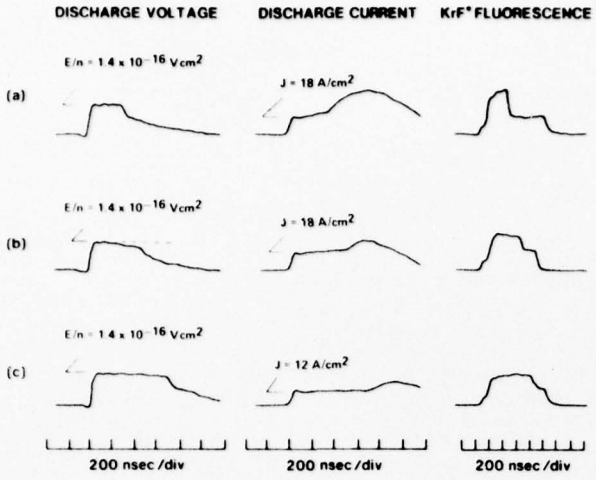

FIG. 2. Measured discharge characteristics for the mixture and e-beam ionization rate of Fig. 1. (a) E/n constant at 1.4×10^{-16} V cm^2; (b) capacitance of driving circuit reduced resulting in temporal reduction in E/n similar to that of curve (b) in Fig. 1; E/n constant at 1.4×10^{-16} V cm^2 with 0.05% NF_3 added.

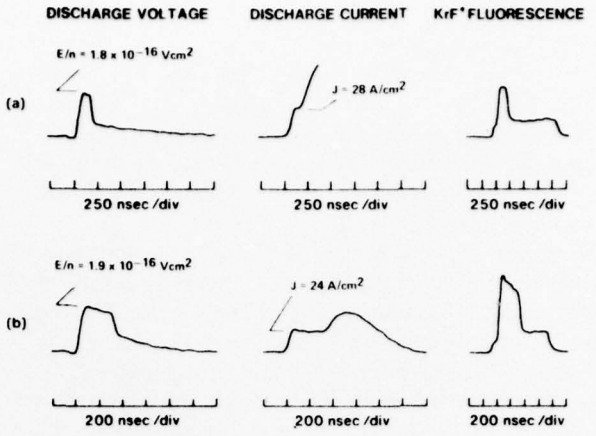

FIG. 3. Measured discharge characteristics for the mixture and e-beam ionization rate of Figs. 1 and 2. (a) E/n constant at 1.8×10^{-16} V cm^2; (b) temporal reduction in E/n from an initial value of 1.9×10^{-16} V cm^2 with 0.025% NF_3 added.

provement in discharge stability as measured by the temporal evolution of the current density is again readily apparent, with the computed energy deposited in the gas approximately twice as large as in the absence of NF_3 [curve (a)]. In addition, average medium properties are comparable to those of curve (b). Numerous calculations carried out on the basis of a tailored e-beam ionization source, as well as a variety of combinations of the techniques outlined above, produced results generally similar to those of Fig. 1.

The stability enhancement techniques described above were investigated experimentally using an e-beam-controlled discharge[2] having an active volume $1.5\times2.0\times50$ cm. Presented in Fig. 2 are discharge current density, voltage, and KrF* fluorescence traces for an Ar(0.95)-Kr(0.05)-F_2(0.005) mixture at 1 atm. The data of Fig. 2(a) correspond to a constant E/n value of 1.4×10^{-16} V cm^2 and exhibit the onset of instability approximately 0.3 μsec after discharge initiation, as indicated by the characteristic sharp rise in current density accompanied by a decrease in both voltage and KrF* fluorescence. The effect of discharge voltage tailoring was evaluated by changing the discharge driving capacitance from 0.9 to 0.5 μF, which resulted in a nearly linear decrease in E/n from an initial value of 1.4×10^{-16} V cm^2 in a manner similar to that corresponding to curve (b) in Fig. 1. Figure 2(b) shows that, according to predictions, the onset of instability was delayed until about the 0.5-μsec point. The influence of NF_3 addition with constant E/n is represented by the data of Fig. 2(c). The observed reduction in the initial current density level and the increase in stable discharge duration to about 0.7 μsec are also found to be in good agreement with analytical predictions.

Figure 3(a) shows that an increase in the constant E/n level to 1.8×10^{-16} V cm^2 for the indicated Ar/Kr/F_2 mixture resulted in instability onset in a time less than 0.1 μsec. However, upon introduction of 0.025% NF_3 ($NF_3/F_2 = 0.05$) and by reduction of the discharge driving capacitance from 10.0 to 0.25 μF in order to produce a temporal decrease in E/n, the stable pulse duration was increased to about 0.35 μsec. For these conditions the discharge power density was 117 kW cm^{-3} and the e-beam power deposition density was 16 kW cm^{-3} (corresponding to an e-beam current density of 2.0 A cm^{-2}). Thus, the discharge energy enhancement factor was about 7. Code calculations for these conditions indicate a zero-field gain of 3.4% cm^{-1}, volumetric absorption of 0.2% cm^{-1}, and KrF* formation efficiency of 25%, values compatible with efficient high-power laser operation.[4]

The stability enhancement techniques described herein are relatively simple to implement and offer the promise of efficient scalable rare-gas–halide and metal-halide lasers at significantly reduced e-beam current density levels, thereby facilitating operation at high average power. At the present time a more complete reporting of this research is in preparation and work with other excimer lasers is underway.

The authors wish to thank R. Preisach for his excellent technical assistance with the experimental portion of the work.

[1] J.D. Daugherty, J.A. Mangano, and J.A. Jacob, Appl. Phys. Lett. **28**, 581 (1976).
[2] R.T. Brown and W.L. Nighan, Appl. Phys. Lett. **32**, 730 (1978).
[3] W.L. Nighan, IEEE J. Quantum Electron. **QE-19**, 714 (1978), and references cited therein.
[4] M. Rokni, J.A. Mangano, J.H. Jacob, and J.C. Hsia, IEEE J. Quantum Electron. **QE-14**, 464 (1978).

Papers

Plasma Processes in Electron-Beam Controlled Rare-Gas Halide Lasers

WILLIAM L. NIGHAN

(*Invited Paper*)

Abstract—**This paper presents the results of an analysis of plasma properties in an electron-beam controlled KrF* laser discharge. In this study, special emphasis is placed on establishing the relationship among the numerous kinetic processes influencing the populations of excited species in the laser medium. Important reactions controlling the coupled populations of rare-gas metastable states and higher excited states are discussed in detail, along with the resultant effect of these reactions on KrF* formation efficiency. It is shown that the rare-gas monohalide production efficiency is approximately 20 percent under typical conditions, and that no single reaction dominates either production or loss of KrF*. In addition, the very important role of halogen molecule dissociation is treated and the resultant effects of dissociation on the temporal variations of plasma properties and on plasma stability are analyzed.**

I. Introduction

THE ELECTRICALLY excited rare-gas halide laser is the first *short-wavelength* laser which appears capable of scaling to high pulse energy and high average power. Electrical-optical energy conversion efficiency of approximately 10 percent has been attained [1] for a single-pulse KrF* laser (λ = 248 nm), the most efficient of the rare-gas halide class. There are numerous applications for efficient UV and/or visible wavelength lasers, and for this reason these new laser systems have become the subject of increasing attention [2]. At the time the potential of rare-gas monohalides as laser molecules was first recognized [3], their properties were essentially unknown. For this reason early emphasis was placed on development of a thorough understanding of the structure of such molecules and their reaction kinetics. These efforts have resulted in a relatively complete understanding of rare-gas halide emission spectra [4], and of the dominant formation and quenching processes of these molecules [5]. Additionally, detailed modeling of kinetic processes has provided the insight required to identify optimum conditions for rare-gas halide laser operation [1], [6], [7].

The plasma medium typical of these lasers is created in a near atmospheric pressure rare-gas mixture containing a small (<1 percent) fractional concentration of a halogen-bearing molecule. Pulsed electrical excitation is provided either by a beam of high energy electrons or by an electric discharge in a manner generally similar to that typical of CO_2 lasers [8], [9]. However, there are several significant features which differentiate rare-gas halide lasers from their IR molecular laser counterparts. These include: 1) a high concentration of "alkali-like" rare gas metastable atoms which, because of their chemical activity [3], exert a dominant influence on all aspects of plasma behavior; 2) a major constituent (the molecular halogen) which dissociates rapidly under the conditions required for laser operation, an effect resulting in very important temporal changes in the gas mixture; and 3) an electron density which is above the level at which electron-electron collisions become important, with the result that the plasma cannot be considered *weakly* ionized. This paper presents the results of a theoretical investigation of these and related plasma processes for conditions representative of KrF* lasers. Special emphasis is placed on establishing the relationship among the numerous kinetic processes which influence the populations of various excited species. The results presented are qualitatively similar for all rare-gas halide lasers, and should provide useful information relevant to other promising excimer lasers as well.

Section II summarizes the basic processes contributing to the production and loss of rare-gas metastable atoms and of KrF* molecules. Particular emphasis is placed on analysis of electron-atom excitation and ionization, especially the dependence of rate coefficients for these processes on the fractional concentration of electronically excited species and of electrons. In addition, the potential importance of vibrational excitation and dissociation of F_2 by low energy electron impact and of electron attachment to vibrationally excited F_2 are discussed.

Manuscript received June 26, 1978. Portions of this work were supported by the Office of Naval Research.

The author is with the United Technologies Research Center, East Hartford, CT 06108.

0018-9197/78/1000-0714$00.75

The results of an analysis of plasma properties in an electron-beam controlled KrF* laser discharge are presented in Section III. Therein the important reactions controlling the coupled populations of rare-gas metastable states and higher excited states are discussed in detail along with the resultant effect of these reactions on KrF* formation efficiency. In addition, the very important role of halogen molecule dissociation is treated and the resultant effect of dissociation on plasma stability is analyzed. Important processes requiring improved understanding prior to successful application of rare-gas halide lasers are discussed in Section IV.

II. Plasma Processes

A. KrF* Formation and Loss

Rare-gas halide lasers have been excited successfully both by electron beams and by electric discharges [1]. In the latter case either fast pulse discharges or electron-beam controlled discharges have been used. Rare-gas monohalide molecule formation proceeds by way of generally similar processes in each case. The more important features of the KrF* formation and loss sequence in a nominally atmospheric pressure Ar-Kr-F_2 gas mixture are illustrated by the diagram shown in Fig. 1. This figure indicates that there are several pathways resulting in the formation of KrF*. When pure electron-beam excitation is used, the dominant mechanisms are two- and three-body positive and negative ion recombination, the positive ions having been produced by ionization initiated by the high energy primary electrons in the beam, and the negative ions by dissociative attachment reactions involving low energy electrons and F_2. Reactions between F_2 and rare-gas metastable atoms produced by low energy electron impact are the primary source of rare-gas monohalide molecules in electron-beam controlled discharges. Recombination and metastable reactions may make comparable contributions to rare-gas halide formation in fast pulse, self-sustained laser discharges, depending on specific circumstances. Of course there are numerous reactions which tend to interrupt the chain of events illustrated in Fig. 1. Nonetheless, the energy utilization efficiency associated with rare-gas monohalide molecule formation is typically in excess of 20 percent for conditions representative of both electron-beam excited and electron-beam controlled lasers [1]. However, electron-beam controlled-discharge excited lasers, for which most of the energy is provided by the discharge, have greater potential for scaling to high average power than lasers excited by an electron-beam alone.

Fig. 1 indicates that there are several processes contributing to the loss of KrF*; these are also found to be of comparable importance for typical conditions. In subsequent paragraphs, specific details of the reactions indicated in Fig. 1 will be discussed with emphasis directed toward factors of importance in discharge excited KrF* lasers.

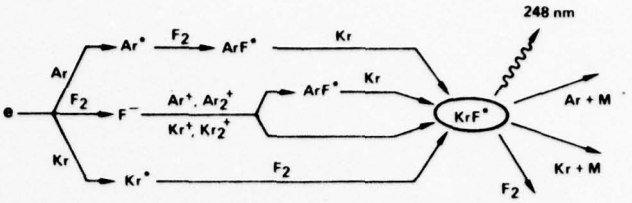

Fig. 1. Illustration of the primary reactions contributing to KrF* formation and loss in an electrically excited Ar-Kr-F_2 mixture at nominally atmospheric pressure.

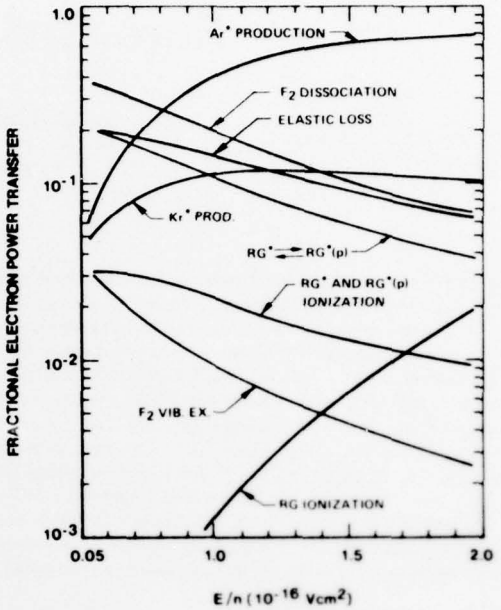

Fig. 2. Fractional contributions to electron-neutral power transfer in an Ar-Kr-F_2 mixture having the proportions 0.945-0.05-0.005. For this example, the fractional ionization, fractional metastable concentration, and fractional concentration of rare gas p state atoms were 10^{-6}, 10^{-5}, and 10^{-6}, respectively. The notation RG refers to the combined effect of Ar and Kr.

B. Electron Collision Processes

Electron-Neutral Energy Transfer: A fundamental factor contributing to the high efficiency characteristic of discharge excited rare-gas halide lasers is the efficient production of rare-gas metastable atoms for conditions readily attainable experimentally. Shown in Fig. 2 are the computed variations of the processes dominating electron-atom (molecule) energy transfer for conditions typical of an electron-beam controlled KrF* laser. For E/n values[1] greater than approximately 1.0×10^{-16} V · cm^2, for which the mean electron energy[2] is about 3.25 eV for the mixture indicated, the combined argon and krypton metastable production efficiencies exceed 50 percent, and reach 70 percent for higher E/n values. Examination of Fig. 2 indicates that the contributions to the undesirable loss of electron energy due to elastic collisions with atoms, excitation of metastable atoms to higher states, and F_2 dissociation are found to be of comparable importance for the conditions of this example. However, it will be shown that the net effect of electron excitation and deexcitation of rare-gas atoms between their metastable and p states is highly variable, depending on the concentration of metastable atoms. For fractional metastable concentrations greater than the 10^{-5} value typical of this ex-

[1] E/n is the ratio of electric field intensity to total neutral number density.

[2] Mean electron energy as used here is defined as $\frac{3}{2}$ the average energy.

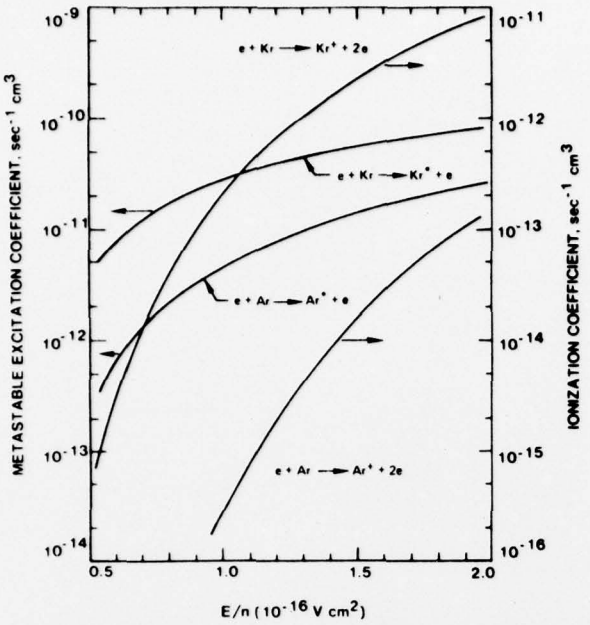

Fig. 3. E/n variation of the metastable excitation and ionization rate coefficients for ground state Ar and Kr corresponding to the conditions of Fig. 2.

ample, the power loss accompanying this process increases significantly [6], [10]. Although the energy loss associated with ionization of excited states and of ground state atoms is small, these processes make very important contributions to the production of electrons in electron-beam controlled discharges.

Even though the cross sections for electron excitation of F_2 vibrational levels are relatively large ($\sim 10^{-17}$ cm^2) [11], vibrational excitation does not appear to be an important *energy loss* process because the energy loss per collision is small ($\sim$0.1 eV) [12]. Although there are no electron cross section data for F_2 electronic excitation, this process may be important because the electron energy loss will be several electron volts. Additionally, there are numerous F_2 electronic states in the 3 to 10 eV range which are repulsive [13] and which would therefore result in F_2 dissociation when excited. In this energy range, there are likely to be excited states of the F_2^- ion which lie above dissociating states of F_2 in the vicinity of the F_2 equilibrium internuclear separation. Thus, for electron energies of a few electron volts F_2 electronic excitation may be enhanced by resonance processes as is the case with dissociative attachment [14]-[16]. In order to reasonably account for the effect of F_2 electronic excitation, indirect experimental evidence of F_2 dissociation has been analyzed, from which an effective $e - F_2$ dissociation cross section has been obtained [12]. Based on this provisional cross section, the data of Fig. 2 show that electron energy loss accompanying direct dissociation by electrons is likely to be substantial for halogen molecule concentrations typical of rare-gas halide lasers. In addition, the contribution of this process to F_2 dissociation will also be shown to be significant.

Electron Rate Coefficients: Presented in Fig. 3 is the E/n variation of the electron rate coefficients for metastable excitation and ionization from the ground state corresponding to the conditions of Fig. 2. These data were generated using available cross section information [17], [18]. With a mean electron energy much lower than the threshold for excitation, only those electrons in the high energy region of the electron energy distribution participate in the metastable production and ionization processes. This accounts for the characteristically strong dependence of the rate coefficients for these processes on E/n (i.e., mean electron energy). The higher rate coefficients for Kr reflect the fact that the energy thresholds for excitation and ionization of krypton are lower than the respective thresholds for argon.

In most if not all electronically excited excimer lasers, the fractional ionization exceeds 10^{-6} and the fractional metastable concentration exceeds 10^{-5}. For these circumstances, electron-electron [19], [20] collisions and electron collisions with metastable atoms [6] exert an important influence on the electron energy distribution, the former tending to increase the number of high energy electrons and the latter resulting in a decrease in their number. Those electron rate coefficients which are particularly sensitive to the high energy region of the distribution are most affected by such changes. Thus, in addition to their strong dependence on E/n, the rate coefficients for electronic excitation and ionization of ground state rare gas atoms exhibit a significant dependence on degree of ionization and on fractional metastable concentration. The results presented in Figs. 4 and 5 illustrate this effect for representive KrF* laser conditions. The influence of electron-electron collisions is particularly striking (Fig. 4), resulting in nearly a two order-of-magnitude increase in the rate coefficient for Kr ionization and a three order-of-magnitude increase for Ar as the fractional ionization increases in the 10^{-6} to 10^{-4} range typical of rare-gas halide discharges.

Fig. 5 indicates that variations in rare gas excitation and ionization rates caused by *cooling* of the electron energy distribution due to excitation of metastable atoms to higher levels are also significant. Of more importance is the fact that since fractional ionization and fraction metastable concentration generally increase together, the effects illustrated in Figs. 4 and 5 tend to be partially offsetting. In addition, the variation shown in these figures for a fixed E/n value of 1.0×10^{-16} V $\cdot$ cm^2 becomes greater as E/n is reduced below this level and is smaller for higher E/n values. Thus, in modeling rare-gas halide laser discharges, it is necessary to evaluate rate coefficients for ionization and excitation from the ground state using self-consistent combinations of E/n, degree of ionization, and metastable fraction.

Presented in Fig. 6 are the E/n variations of the rate coefficients for Ar and Kr excitation and deexcitation between the grouped metastable and p states, calculated using available cross section data [21]. Rate coefficients for ionization from both the metastable and p states are also shown [22], [23]. These data exhibit a weak dependence on E/n, reflecting the fact that the energy thresholds for the processes involved are comparable to (or less than) the mean electron-energy. For this reason the rate coefficients presented in Fig. 6 are practically insensitive to variations in either the degree of ionization or the metastable fraction. However, the magnitude of the rate coefficients for electron-excited state collision processes is exceptionally large as a consequence of the alkali-like structure of the rare-gas excited states [21].

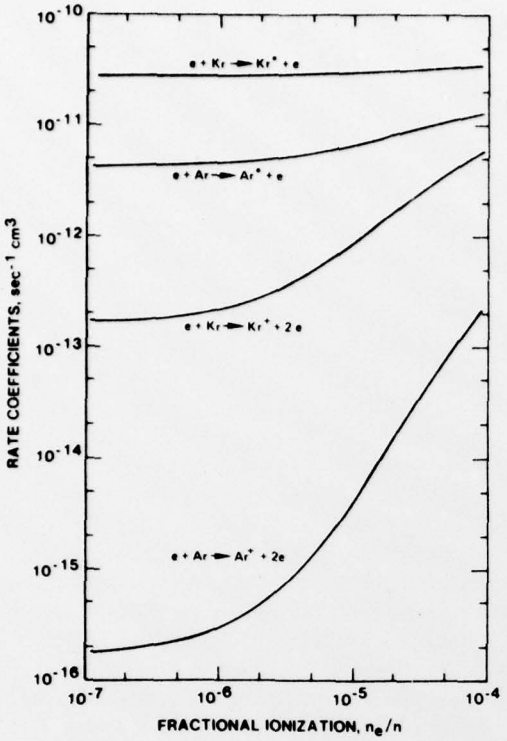

Fig. 4. Variation of Ar and Kr rate coefficients for metastable production and ionization with fractional ionization for an E/n value of 1.0×10^{-16} V · cm^2. The fractional concentrations of metastable and p state atoms were fixed at 10^{-5} and 10^{-6}, respectively.

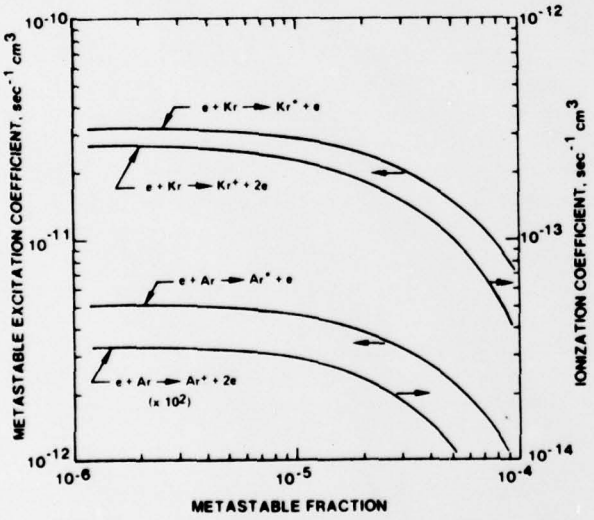

Fig. 5. Variation of Ar and Kr rate coefficients for metastable production and ionization with metastable fraction for an E/n value of 1.0×10^{-16} V · cm^2 and a fractional ionization of 10^{-6}. The fractional p state concentration was increased in proportion to the metastable fraction so that the p state: metastable ratio was always 0.1.

F_2 Vibrational Excitation: Fig. 6 also shows the electron rate coefficients for F_2 vibrational excitation and for dissociative attachment of F_2 in the vibrational ground state and in the first vibrational level, computed using the theoretical cross sections of [11]. The rate coefficient for vibrational excitation reflects excitation from the ground state to the first ten

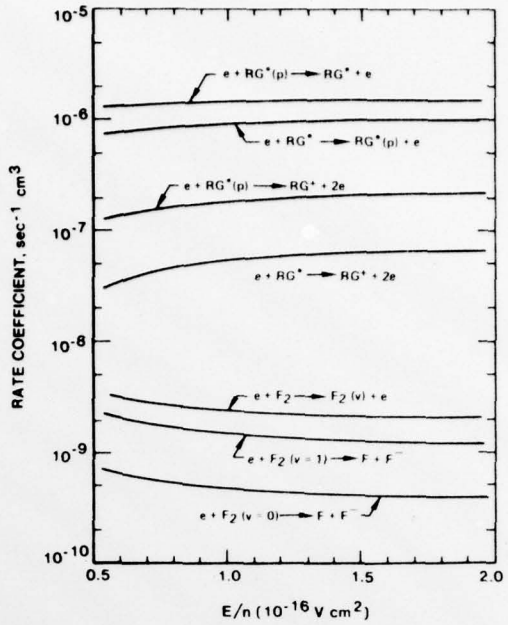

Fig. 6. E/n variation of electron rate coefficients for excitation, deexcitation and ionization of rare gas p state atoms, along with the rate coefficients for metastable ionization, F_2 dissociative attachment, and F_2 vibrational excitation. The rate coefficients for these processes exhibit very little change in response to variations in fractional ionization or excited state concentration. The notation RG refers to either Ar or Kr.

vibrational levels, each of which has been energy weighted [24] with respect to the first level. The attachment rate coefficient for F_2 in the ground vibrational level is found to be within 5 percent of that computed using recent experimental cross section data [16]. While attachment cross sections for vibrationally excited F_2 have not been measured, this agreement lends support to the theoretical prediction [11] that attachment to vibrationally excited F_2 should proceed at a much faster rate than for $F_2(v = 0)$. If such is the case, the increasing population of vibrationally excited F_2 during the discharge excitation pulse will result in an increase in electron loss due to attachment, thereby tending to offset the reduction in the attachment loss accompanying the loss of F_2 due to dissociation. Subsequent discussion will show that such an effect could influence the onset of plasma instability.

C. Excited State Processes

In addition to efficient rare gas metastable production, efficient rare-gas monohalide formation requires that reactions leading to the formation of KrF* dominate over competing metastable quenching processes. Thus, reactions between rare-gas metastable atoms and the halogen "fuel" molecule must be the dominant metastable loss process; and the branching ratio for the formation of the desired rare-gas monohalide molecule must be near unity. Setser and co-workers [25] have conducted extensive investigations of rare-gas metastable atom quenching and have found that practically all halogenated molecules have large rate constants. Moreover, diatomic halogens such as F_2 have near unity branching ratio for rare-gas monohalide formation. Thus, energy efficient formation of

rare-gas monohalide molecules is usually assured in discharges in which rare-gas metastables are produced efficiently, and in which an appropriate halogen fuel molecule is present.

With a stimulated emission cross section in the 1 to 5×10^{-16} cm^2 range [1], maintenance of optimum gain requires a rare-gas monohalide density of about 10^{14} cm^{-3}, a relatively high excited state concentration even for an atmospheric pressure glow discharge. Thus, knowledge of rare-gas halide loss mechanisms under various conditions is particularly important. The dominant rare-gas halide quenching processes have been identified by Rokni, Jacob, and Mangano whose detailed analysis and interpretation is presented elsewhere [5]. Certain of their results relevant to KrF* lasers are summarized in Table I along with other related data [26]-[30]. It is worth pointing out that each of the major constituents in the gas mixture collisionally quenches [5] KrF* (Fig. 1, Table I). Additionally, with a radiative lifetime less than 10 ns, spontaneous decay of the rare-gas monohalide laser molecule is always important for the conditions of interest.

Quenching of Rare-Gas P State Atoms by Neutral Collisions: Fig. 6 shows that the rate coefficient for electron impact excitation of rare-gas metastable atoms to the higher lying manifold of p states [21] is very large. Indeed, for the conditions encountered in rare-gas halide lasers, this process can compete with the desired metastable-F_2 rare-gas monohalide formation channel. Thus, the significance of p state excitation from the metastable state depends on what happens to the p-state atoms after they are produced. For this reason, a knowledge of p-state quenching processes is particularly important. Recently Chang and Setser [30] reported rate coefficients for collisional quenching of Ar p-state atoms by argon at room temperature (Table I). Their results show that metastable production as a result of p-state quenching by ground state atoms will be very fast for pressures typical of rare-gas halide lasers. Such p-state-metastable transitions can be explained [30] in terms of a curve crossing mechanism among the Ar_2^* repulsive states which then dissociate, e.g., $Ar^*(p) + Ar \rightarrow Ar_2^* \rightarrow Ar^* + Ar$. Subsequent discussion will show that this process can dominate p-state atom quenching in rare-gas halide lasers thereby exerting an important influence on both rare-gas halide formation efficiency and plasma stability.

TABLE I
RARE GAS AND RARE-GAS HALIDE NEUTRAL REACTIONS AND RATE COEFFICIENTS FOR KrF* LASERS

Reaction	Rate Coefficient[a]	Reference
$Ar^* + Kr \rightarrow Kr^*(p) + Ar$	5.6 (-12)	26
$Ar^* + F_2 \rightarrow ArF^* + F$	7.5 (-10)	5
$Kr^* + F_2 \rightarrow KrF^* + F$	7.8 (-10)	5
$Ar^*(p) + Ar \rightarrow Ar^* + Ar$	2-6 (-11)	30
$Kr^*(p) + Ar \rightarrow Kr^* + Ar$	2-6 (-11)	estimated (see 30)
$ArF^* + Kr \rightarrow KrF^* + Ar$	1.6 (-9)	5
$ArF^* + Ar + M \rightarrow Ar_2F^* + M$	4.0 (-31)	5
$KrF^* + Kr + M \rightarrow Kr_2F^* + M$	6.5 (-31)	5
$KrF^* + 2Ar \rightarrow$ products	7.0 (-32)	5
$ArF^* + F_2 \rightarrow$ products	1.9 (-9)	5
$KrF^* + F_2 \rightarrow$ products	7.8 (-10)	5
$KrF^* \rightarrow Kr + F + h\nu$ (248 nm)	9 (-9)	27
$ArF^* \rightarrow Ar + F + h\nu$ (193 nm)	$\sim$ 4 (-9)	29
$Kr_2F^* \rightarrow 2Kr + F + h\nu$ (400 nm)	181 (-9)	28
$Ar_2F^* \rightarrow 2Ar + F + h\nu$ (290 nm)	132 (-9)	29

[a] Units: two-body processes, sec^{-1} cm^3; three-body processes, sec^{-1} cm^6; radiative processes, sec. The number in ( ) refers to the exponent of ten.

III. Laser Discharge Analysis

A. Temporal Variations

Plasma Modeling: Analysis of plasma properties in pulsed rare-gas halide lasers requires modeling of the time dependent variation of electron, ion, and excited state processes for conditions typical of the excitation scheme of interest [1], [6], [7]. In the present work, emphasis has been placed on electron-beam controlled laser discharges operating under conditions similar to those described in [31]. For the most part, the modeling procedures used are similar to those typically employed in such analyses [6], [7]. The principle electron and excited state reactions and rate coefficients used in the present analysis have been discussed in the preceding section and are presented in Figs. 3-6 and in Table I. The dependence of electron-atom rate coefficients on variations in E/n, fractional ionization and metastable fraction was accounted for by solving the Boltzmann equation [19], [24] in order to generate a matrix of data similar to those presented in Figs. 3-5. On the basis of the data so obtained, rate coefficients for excitation and ionization from the ground state were represented analytically by an expression of the form,

$$k(E/n, \alpha, \delta) \equiv k_0(E/n) f(E/n, \alpha) g(E/n, \delta),$$

where k is the rate coefficient for a particular process, α is the fractional ionization, δ is the metastable fraction, and f and g are E/n dependent analytic functions reflecting the numerically determined variations in k with changes in α and δ (Figs. 4 and 5). Thus, k_0 was determined by specifying an E/n value in the range of interest. The rate coefficients $k(E/n, \alpha, \delta)$ were then computed as a function of time using self-consistent values of α and δ.

Species Concentrations: Fig. 7 presents the computed temporal variation of selected species for representative experimental conditions [31]. In this example, the external ionization source was increased as a function of time in order to simulate the increase in *e*-beam current density typical of pulsed, cold-cathode *e*-gun operation [31]. For these conditions, plasma properties reach quasi-steady values in a time less than 0.1 μs. However, Fig. 7 shows that significant changes occur on a longer time scale because of the combined influence of the increasing *e*-beam ionization rate and F_2 dissociation, particularly the latter. Indeed, for this example F_2 dissociation exceeds 25 percent after about 0.6 μs. The results presented in this figure show that the fractional ionization ($\alpha = n_e/n$) and metastable fraction ($\delta = n^*/n$) are approximately 4×10^{-6} and 10^{-5}, respectively, values for which electron rate coefficients are affected by collisions with other electrons and with metastable atoms (Figs. 4 and 5). In addition, Fig. 7 shows

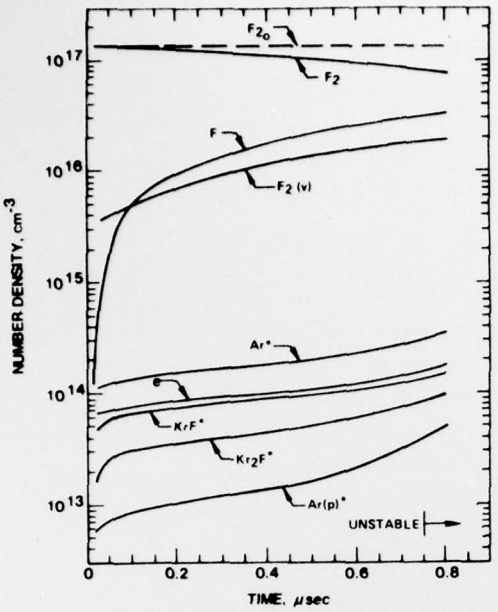

Fig. 7. Temporal variation of selected species in an *e*-beam controlled KrF* laser discharge at a pressure of 1 atm; Ar–Kr–F_2 (0.945–0.05–0.005). For this example the E/n value was 1.2×10^{-16} V · cm^2; and the temporal variation of the *e*-beam ionization rate was $160 + 8 \times 10^7 t$ s^{-1}, resulting in a 50 percent increase in the electron production rate after 1 μs.

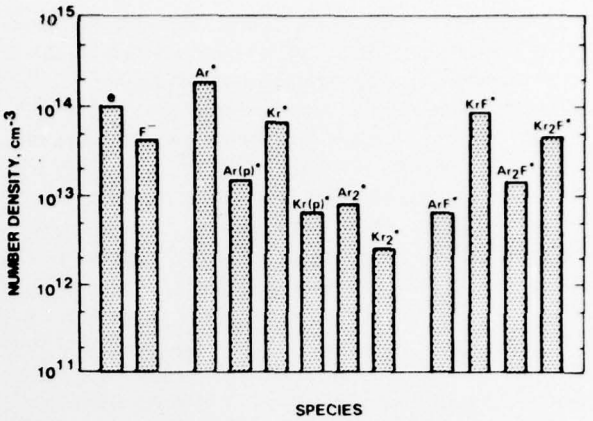

Fig. 8. Particle concentrations corresponding to the conditions of Fig. 7 at a time 0.4 μs after discharge initiation.

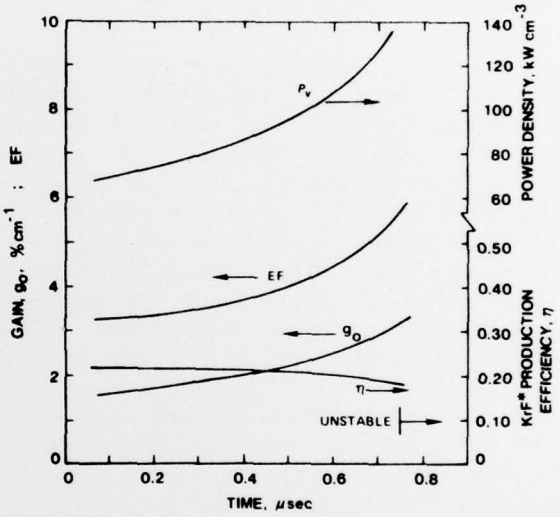

Fig. 9. Temporal variation of total electrical power density (P_v), discharge: *e*-beam power enhancement factor (EF), small-signal gain (g_0), and KrF* production efficiency (η) for the conditions of Fig. 7.

that after a few tenths of a μs the concentrations of vibrationally excited F_2 and of F atoms reach levels corresponding to about one-tenth the initial F_2 density.

The computed populations of all excited species considered in the present analysis are presented in Fig. 8 for a time 0.4 μs after discharge initiation. This figure shows that the primary excited species are the rare gas metastables, Ar* and Kr*, and the krypton-fluorides KrF* and Kr_2F*, each having a concentration of approximately 10^{14} cm^{-3}. Other excited species have number densities in the 2×10^{12}–2×10^{13} cm^{-3} range, with the total excited state fraction in excess of 2×10^{-5} for the conditions of this example. Clearly there are other excited rare gas and rare-gas halide molecules which will probably have concentrations on the order of 10^{12} cm^{-3} for conditions typical of rare-gas halide lasers.

Medium Properties: Numerical modeling of laser characteristics begins with a study of microscopic processes, analysis of which is the primary source of insight required to optimize and/or improve conditions. However, an equally important objective of such studies is quantitative computation of macroscopic properties of the laser medium which can be directly compared with experimental results. Indeed, comparison between predicted and measured rare-gas halide laser characteristics has been found to be very good [1], [7], [31].

Fig. 9 shows the computed small-signal gain, KrF* production efficiency, total volumetric power density, and discharge: *e*-beam power enhancement factor corresponding to the conditions of Figs. 7 and 8. The KrF* production efficiency (η) as used here includes the quantum efficiency and as such represents the fraction of the total power potentially available for conversion to optical power. The enhancement factor (EF) is simply the ratio of the discharge power to that supplied by the *e*-beam. The data of this figure illustrate the high gain and remarkable rare-gas monohalide production efficiency characteristic of rare-gas halide lasers, KrF* in particular. Note, however, that although the power density is dominated by the discharge contribution (EF > 1), the enhancement factor is very much lower than that typical of IR molecular lasers [9]. This is a direct consequence of the high *e*-beam power required to maintain the electron density at the necessary level in the presence of the enormous loss rate of electrons due to F_2 dissociative attachment, a circumstance resulting in significant practical problems related to certain aspects of electron-beam technology. Furthermore, with a total electrical power density of approximately 100 kW · cm^{-3}, the rate of gas temperature rise is well over 100 K per μs. This factor, when considered along with the rate of loss of fluorine fuel due to dissociation (Fig. 7), establishes an upper limit for laser pulse duration which is on the order of a few μs.

Fig. 9 shows that the energy utilization efficiency associated

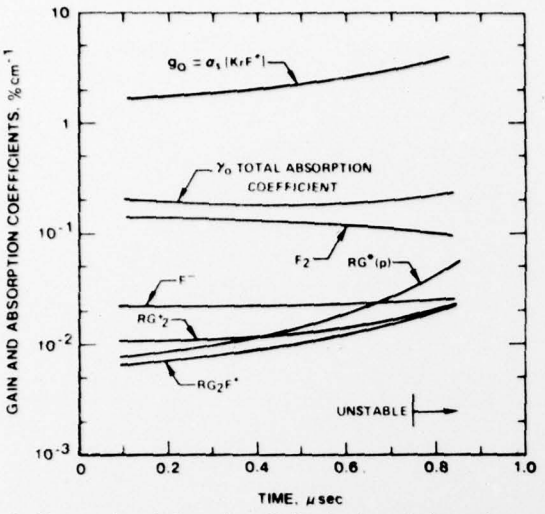

Fig. 10. Temporal variation of small-signal gain and absorption coefficients for the conditions of Fig. 7. The KrF* stimulated emission cross section used was 2.4×10^{-16} V · cm^2; and the absorption cross sections used for the species indicated were those reported in [32]. In this figure the notation RG refers to the combined effect of Ar and Kr.

with KrF* production can be very high (~20 percent). However, overall laser efficiency is also dependent on optical power extraction efficiency. Analysis shows that optical extraction efficiency can be significantly affected by the presence of electronically excited and/or ion species which absorb at the UV laser wavelength [1], [32], even though the absorption coefficient (γ_0) may be less than one-tenth as large as the gain coefficient. Indeed, it has been shown [1] that efficient optical extraction requires that $\gamma_0/g_0 < 0.1$. Presented in Fig. 10 is the computed temporal variation of the total absorption coefficient at the KrF* laser wavelength (248 nm) corresponding to the conditions of Fig. 7. Also shown are the individual contributions from known absorbing species, computed on the basis of reported cross section data [32]. For the conditions of this example, photodissociation of F_2 is obviously the dominant laser absorption process. However, the concentrations of ionic and excited species are subject to much greater variation than the F_2 density, and their combined influence is very significant as indicated in Fig. 10. Analysis of optical extraction efficiency for the conditions of this figure yields a value of about 45 percent for an active medium length of 1 m. When combined with a KrF* production efficiency of 20 percent (Fig. 9), an electrical-to-optical conversion efficiency of almost 10 percent is indicated, in accord with the highest experimental values attained to date under similar conditions [1].

B. Dominant Processes

As indicated in Section II, numerous processes must be considered in the analysis of rare-gas halide lasers. However, numerical experimentation shows that certain processes such as rare gas metastable loss tend to be dominated by a single reaction. Others such as KrF* formation and loss are affected by several reactions of approximately equal importance. Examination of the relative importance of the various coupled reactions is useful and provides insight helpful to understanding and improving rare-gas halide lasers. In the following paragraphs, the relative contributions to electron production, metastable and p state loss, and KrF* production and loss for the conditions of Figs. 7-9 will be discussed.

Electron Production: Ideally, when electron-beam ionization is employed to provide a stable, large volume plasma medium, ionization is controlled entirely by the external ionization source, effectively decoupling electron production from other plasma properties. Such is the case in IR molecular lasers [9], for example, in which the mean electron energy required for efficient vibrational excitation is much less than that for which electronic excitation and ionization become significant. However, in rare-gas halide lasers (and other excimer lasers as well) the mean electron energy required is several electron volts and the density of electronically excited species is high [9]. Given these circumstances along with the alkali-like structure of rare-gas metastables, significant ionization by low energy plasma electrons is usually unavoidable even when an external ionization source is used.

Fig. 11 compares the various fractional contributions to electron production in a KrF* laser discharge operating under the conditions of Fig. 7. These results show that although ionization by the high energy *e*-beam is dominant, low energy electron impact ionization of rare-gas metastable atoms provides almost 20 percent of the ionization, a contribution which increases significantly with time. Indeed, even ionization of argon and krypton p states is important for the conditions of this example. The nonnegligible contribution of ground state ionization is a direct reflection of the increase in the ionization rate coefficient caused by electron-electron collisions.

The relative contributions to the ionization process as indicated by Fig. 11 are typical of the *e*-beam controlled rare-gas halide lasers that have been operated to date [1], [31], [33]-[35]. On the basis of these results, it is apparent that such discharges are actually of a hybrid nature in which substantial contributions to ionization are made by both high energy beam electrons and by plasma electrons.

Metastable and p State Loss Processes: In *e*-beam controlled rare-gas halide discharges, production of rare-gas metastable atoms is dominated by a single process, electron impact excitation of ground state atoms. However, there are several reactions by which metastable atoms are lost. Fig. 12 presents a comparison of the Ar* loss processes for the conditions of present interest. The effect of coupling between the metastable and p states has been grouped as a single process as indicated. Thus, $Ar^* \rightleftarrows Ar^*(p)$ represents the net effect of electron excitation of the p states from the metastable states, and transitions back to the metastable states caused by both electron and neutral collisions and by radiative decay. This figure vividly illustrates the dominance of the desired metastable-halogen reaction [25] and in part explains why the KrF* laser is so attractive. Although such selectivity is a requirement for efficient KrF* formation, a consequence of the dominance of the RG^*-F_2 reaction is that the metastable concentration is particularly sensitive to the loss of F_2 due to dissociation. Since metastable ionization makes a significant contribution to electron production (Fig. 11), the increased metastable concentration accompanying dissociative loss of F_2 has a particularly

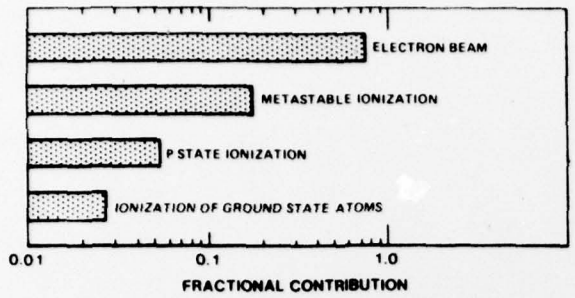

Fig. 11. Fractional contributions to electron production in an *e*-beam controlled KrF* laser discharge for the conditions of Fig. 7. These results, and those presented in Figs. 12, 13, and 15-17, refer to the time 0.4 μs after discharge initiation and are representative of conditions in the 0.2 to 0.6 μs time range.

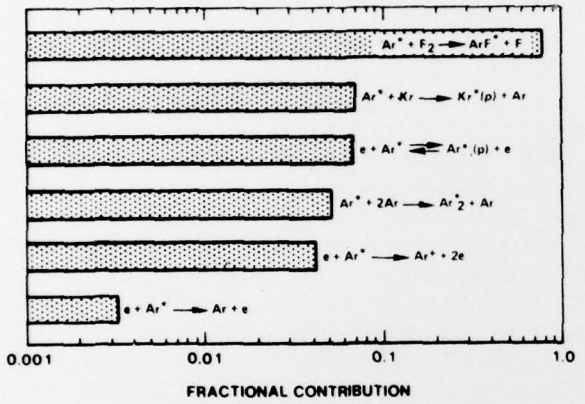

Fig. 12. Fractional contribution to argon metastable loss in an *e*-beam controlled KrF* laser discharge for the conditions of Fig. 7.

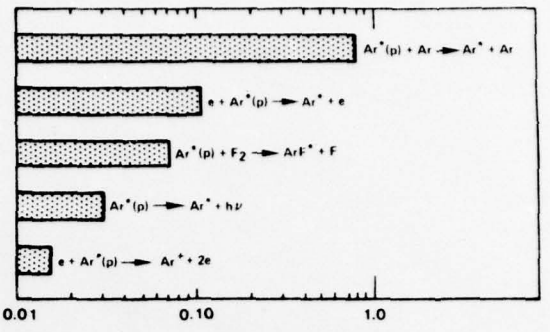

Fig. 13. Fractional contributions to the loss of argon p state atoms in an *e*-beam controlled KrF* laser discharge for the conditions of Fig. 7.

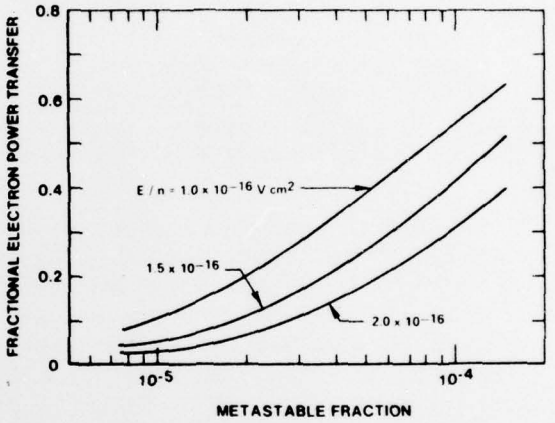

Fig. 14. Fractional loss of electron power resulting from the net effect of excitation and deexcitation of the rare gas p states in an Ar–Kr–F_2 (0.945–0.05–0.005) mixture. The fraction of p state atoms was maintained at a value one-tenth that of the metastable fraction for the purposes of this illustration.

serious effect on plasma stability, a topic which is discussed in a subsequent section.

For the reasons discussed in Section II, knowledge of the processes by which rare gas p state atoms are lost is of considerable importance. There are numerous processes resulting in the loss of p-state atoms including: electron superelastic collisions by which p-state atoms are converted back to metastable states with no net loss of electron energy, halogen reactions,[3] quenching by neutrals which also results in metastable production [30], electron excitation and ionization, and spontaneous radiative transistions back to the metastable states. Presented in Fig. 13 are the relative contributions of these processes to the loss of argon p-state atoms. These results show that neutral quenching of p-state atoms by ground state rare-gas atoms is the dominant p-state loss process. Thus, p-state atoms produced by way of electron collisions with metastable atoms are rapidly converted back to metastables by collisions with ground state atoms, with the result that this process has little net effect on the density of metastable atoms. However, the electron energy expended to produce p-state atoms from metastables is converted to translational energy of neutrals. As long as the electron energy loss associated with production of p-state atoms is not large the laser energy utilization efficiency is not greatly affected by this process. However, Fig. 14 shows that the fractional electron energy loss associated with p-state excitation depends directly on the metastable density and becomes very significant if the metastable fraction exceeds a value of approximately 3×10^{-5}.

KrF Formation and Loss:* The mechanisms responsible for rare-gas halide formation and loss have been the subject of extensive experimentation and analysis [1], [5], [25], [27], [28]. As a result, the reactions of primary importance have been identified and a generally complete set of rate data is available for use in analyses such as that described herein. Figs. 15 and 16 present a comparison of the relative importance of KrF* production and loss for the conditions of Fig. 7. For the conditions of this example, the ArF*-Kr displacement reaction [5] dominates the formation of KrF*. Examination of Figs. 2, 12, and 15 reveals the direct, efficient channel of energy from the electrons to Ar* to ArF*, and finally to KrF*. For typical conditions, the energy channeled through the KrF* molecule represents between 20 and 30 percent of the total discharge energy (Fig. 9). Note, however, that both

[3] In this analysis it has been assumed that p-state-F_2 reactions result in RGF* formation and proceed at a rate equal to that of the corresponding metastable reaction.

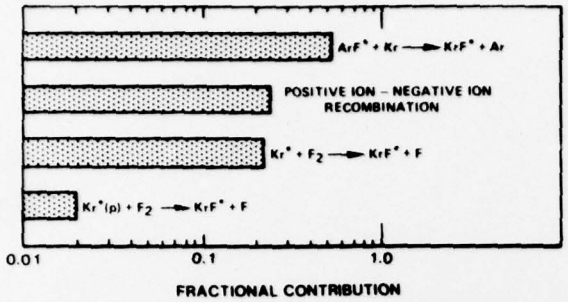

Fig. 15. Fractional contributions to KrF* production in an *e*-beam controlled laser discharge for the conditions of Fig. 7.

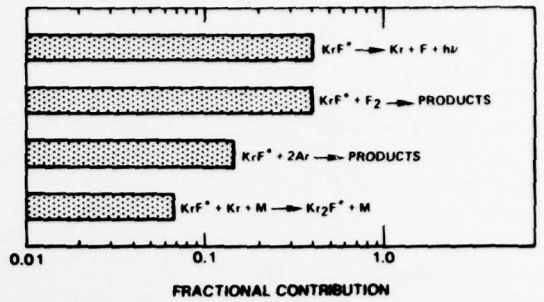

Fig. 16. Fractional contributions to KrF* loss (in the absence of a radiation field) for the conditions of Fig. 7.

the contributions of positive ion-negative ion recombination and of the direct reaction of F_2 with krypton metastables are also significant. The relative importance of the Kr^*-F_2 reaction will be even larger for values of Kr fractional concentration larger than the 0.05 considered here.

For the present case in which there is no optical field present, spontaneous decay and F_2 quenching are both very important loss channels for KrF* as indicated in Fig. 16. However, three-body quenching by Ar and Kr are also very significant. Indeed, for somewhat higher Kr fractions and/or at pressures of a few atmospheres, three-body quenching becomes the dominant KrF* loss process. Under these circumstances the concentration of the triatomic rare-gas halide Kr_2F^* approaches and even exceeds the KrF* density.

Of particular interest is the fact that in *e*-beam controlled, discharge pumped lasers, no single process dominates either production or loss of the diatomic rare-gas halide molecule. Of course, efficient laser operation requires conditions such that stimulated emission is the dominant KrF* loss process. With the ratio of gain to absorption (g_0/γ_0) having a value of about ten, analysis shows that efficient optical power extraction requires an optical flux approximately twice the saturation level [1], the latter having a value of nearly 1 MW · cm^{-2} for the conditions of Fig. 16.

C. F_2 Dissociation

The results and discussion presented above show that optimum conditions for efficient production of KrF* can be achieved in high-power *e*-beam controlled (or *e*-beam excited) lasers. In addition it is shown that F_2 exerts a very important (indeed dominant) influence on the concentrations of electrons, metastable and p-state atoms, and rare-gas halide molecules. Thus, no single process exerts an influence on laser plasma conditions which is comparable to the effects of F_2 dissociation. Fig. 7 shows that substantial F_2 dissociation can occur in a time less than 1 μs in *e*-beam controlled discharges. Although plasma conditions are quite satisfactory for the first 0.5 μs for this example (Fig. 9), as a result of dissociation, a substantial variation in properties occurs for times in excess of about 0.6 μs, resulting in the occurrence of plasma instability shortly thereafter.

The various contributions to F_2 dissociation for these conditions are presented in Fig. 17. By far the most important feature of this figure is its indication of the large number of different processes resulting in dissociation. Clearly, F_2 dissociative reactions are of a fundamental nature in rare-gas halide lasers. Indeed, because of the large number of reactions involved, numerical experimentation shows that the quasi-steady plasma properties discussed in previous paragraphs are relatively insensitive to variations in the rate coefficients used for the reactions indicated in Fig. 17, within known limits of uncertainty. However, since ionization resulting from low energy electron impact is always important (Fig. 11) for the conditions of primary interest, the plasma is only marginally stable. For this reason, the time at which instability actually occurs can vary significantly in response to changes in the F_2 concentration.

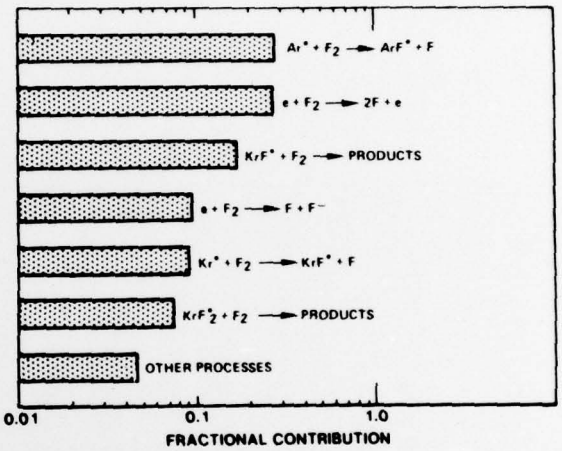

Fig. 17. Fractional contributions to F_2 dissociation in an *e*-beam controlled KrF* laser discharge for the conditions of Fig. 7.

D. Plasma Instability

For the electrical power density values required for optimum laser performance, the loss of F_2 due to dissociation, along with gas heating, establishes a maximum limit for discharge pulse length which is on the order of a few μs. However, the occurrence of plasma instability (current runaway) in a much shorter time actually determines the maximum attainable pulse duration in *e*-beam controlled rare-gas halide lasers [1], [31], [33]-[35]. For this reason, plasma instability plays a

uniquely important role in determining the experimentally accessible range of laser discharge operating parameters, especially discharge: *e*-beam power enhancement factor [1] (Fig. 9).

Electron Density Growth: Completely self-consistent analysis of rare-gas halide laser stability is a formidable problem, requiring consideration of the temporal response of the electrons, ions, and several excited species to disturbances in plasma properties. However, the mode of instability leading to current runaway in rare-gas halide discharges has been identified as ionization instability [1], [31], [36], [37]. This instability is a manifestation of temporal amplification of electron density disturbances. Therefore, useful insight can be obtained by consideration of the time dependent electron conservation equation alone. For the present purpose, this equation may be expressed in the form

$$\frac{\partial n_e}{\partial t} \simeq nS + n_e n k_i + n_e n^* k_i^* + n_e n^*(\mathrm{p}) k_i^*(\mathrm{p}) - n_e n_{F_2} k_a, \tag{1}$$

where n_e, n, n^*, $n^*(\mathrm{p})$, and n_{F_2} are the densities of electrons, ground state neutrals, metastables, p-state atoms and F_2, respectively, S is ionization rate due to the external source, and k_i, k_i^*, and $k_i^*(\mathrm{p})$ are the rate coefficients for ionization of ground state atoms, metastable atoms, and p-state atoms (Figs. 3-6), and k_a is the F_2 attachment rate coefficient. If it is assumed that excited species respond to disturbances on a time scale which is shorter than that of the electrons,[4] and that electron density disturbances vary as exp (υt), application of first-order perturbation theory results in the following approximate expression for the *maximum* growth rate of electron density disturbances:

$$\upsilon \simeq n k_i \left(1 + \frac{\alpha}{k_i}\frac{\partial k_i}{\partial \alpha}\right) + 2n^* k_i^* + 3n^*(\mathrm{p}) k_i^*(\mathrm{p}) - n_{F_2} k_a. \tag{2}$$

The first term on the right-hand side is the contribution of ground state ionization; thus the term $(\alpha/k_i)\partial k_i/\partial\alpha$ is a dimensionless quantity of order unity which reflects the variation in the ionization rate coefficient with changes in fractional ionization α (Fig. 4). The second and third terms reflect the influence of metastable and p-state ionization, respectively, the factor-of-two arising because the metastable concentration varies as the square of the electron density, and the factor-of-three because the density of p-state atoms varies as the cube of the electron density. In order to ensure stability ($\upsilon < 0$, electron density disturbances damped), the attachment term $n_{F_2} k_a$, must always be larger than the combined contributions to (2) from the various ionization processes.

Presented in Fig. 18 are the temporal variations of the dominant contributions to (2) for the conditions of Fig. 7, i.e., excited state ionization and attachment to F_2 (in the ground vibrational state). Initially, conditions are such that the contribution due to ionization from excited states is safely below that due to attachment, the latter effectively balanced by ionization provided by the external source (Fig. 11). However, as the F_2 concentration decreases as a result of dissociation, this situation changes significantly with ionization from excited states increasing by about a factor of two in only a few tenths of a μs. Thus, the criterion for ionization stability ($\upsilon < 0$) is quickly violated, usually in a time less than 1 μs after discharge initiation.

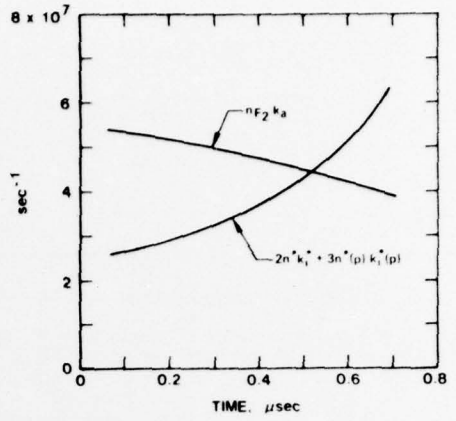

Fig. 18. First-order contributions to the growth (or damping) rate of electron density disturbances resulting from ionization of Ar and Kr excited states and from dissociative attachment to F_2 in the ground vibrational state for the conditions of Fig. 7.

Although the stabilizing influence of attachment is initially about twice as large as the terms due to ionization [(2), Fig. 18], the effects on electron density growth of attachment and ionization become equal ($\upsilon = 0$) as a result of only 25 percent F_2 dissociation (Fig. 7). Analysis of the factors contributing to (2) shows that the ratio of the ionization terms (destabilizing) to the attachment term (stabilizing) varies approximately as $n_{F_2}^{-3}$. For this reason, whenever ionization from excited states becomes significant (>10 percent) relative to that provided by the *e*-beam, plasma stability is exceptionally sensitive to the loss of F_2.

Current Runaway: The temporal evolution of discharge current density prior to instability onset and the time at which current runaway actually occurs are both very sensitive to the discharge E/n value. Fig. 19 presents computed current density profiles for various E/n values and conditions otherwise similar to those discussed previously. The discharge: *e*-beam power enhancement factor at the leading edge of the pulse is also indicated. Although the current density is uniform and the plasma is stable for over 1 μs at an E/n value of 1.0×10^{-16} V · cm^2, at this value the power enhancement factor is only about two. That is, about $\frac{1}{3}$ of the total power is provided by the *e*-beam ionization source just to maintain the electron density at the required level. Increasing E/n results in a substantial increase in the discharge power, and therefore in the enhancement factor as is desired. However, Fig. 19 shows that this is accomplished at the expense of stable discharge dura-

[4] Although electrons and metastable atoms often respond to disturbances on the same time scale, the approximation that perturbations in the metastable concentration are quasi-steady significantly simplifies analysis, thereby facilitating development of insight as regards the causes of ionization instability.

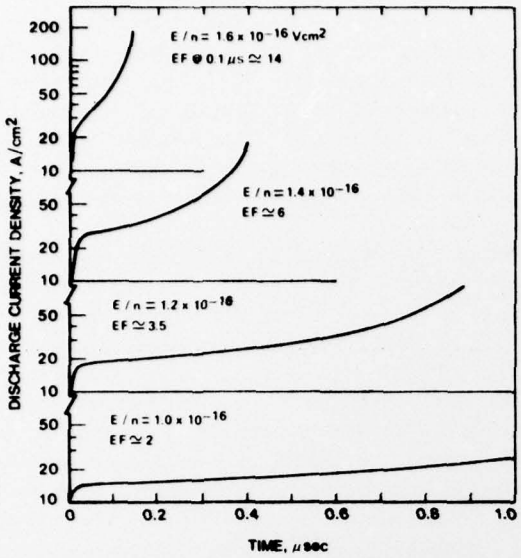

Fig. 19. Temporal variation of discharge current density for various E/n values and conditions otherwise the same as Fig. 7. The indicated values of discharge: *e*-beam power enhancement factor refer to the time 0.1 μs after discharge initiation.

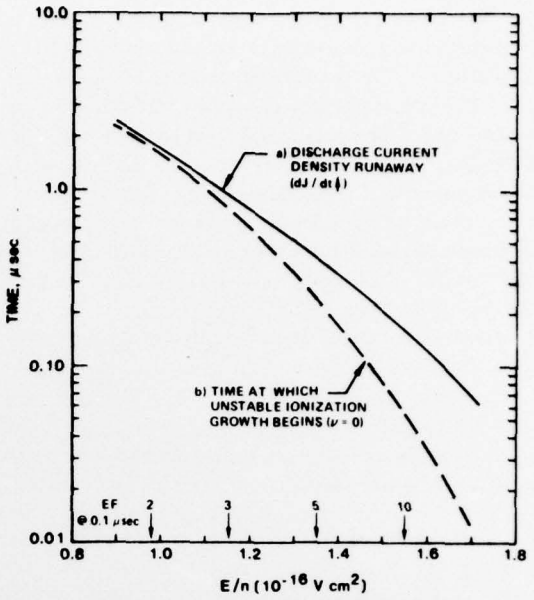

Fig. 20. E/n variation of the time after discharge initiation at which numerically determined current runaway begins (curve *a*); and at which exponential growth of electron density disturbances begins, i.e., ionization instability (curve *b*). In the evaluation of curve *b*(υ = 0) ionization of ground state atoms and attachment of vibrationally excited F_2 were taken into account. These results correspond to the conditions of Fig. 7.

tion. For E/n values of 1.2×10^{-16} V · cm^2 and higher, current density runaway occurs in a time less than one μs as is evidenced by a rapidly increasing current density derivative.

Instability Onset Time: Presented in Fig. 20 is the E/n dependence of the time at which the computed current density runaway occurs as determined by the present kinetic model for KrF* laser conditions. Instability onset time determined on this basis is directly comparable with experimental observation of current runaway; and, the computed current runaway time presented in this figure is found to be in good agreement with measured values [31]. Since current runaway is particularly sensitive to the concentration of rare-gas excited states, for which there is no direct experimental measure, agreement between calculated and measured current density profiles serves as a check on the accuracy of the former. Also shown in Fig. 20 is a dashed curve representing the time after discharge initiation at which the theoretical criterion for ionization instability is first satisfied ($\upsilon = 0$). This time was determined by computing the instability growth (or damping) rate using time varying plasma conditions to evaluate (2). For low values of E/n the plasma is stable for a relatively long time (~1 μs). Under these conditions, the computed instability onset time based on the theoretical criterion ($\upsilon = 0$) and on the current runaway time as determined from the complete kinetics calculation are essentially equivalent, reflecting the very short time (<100 ns) characterizing ionization growth after the initiation of instability.[5] As E/n is increased, the time characteristic of stable discharge duration ($\upsilon < 0$) is reduced dramatically, approaching zero for E/n values only slightly higher than those shown in the figure. That is, for high E/n values, the plasma is unstable practically from the time of its initiation, based on the criterion that υ be less than zero to ensure stability. However, Fig. 20 shows that the actual occurrence of current runaway at high E/n values is delayed by a time which is approximately equal to the ionization growth time, $\sim(n^* k_i^*)^{-1}$. Nevertheless, for the conditions considered here, the duration of the excitation pulse for which the energy enhancement factor can be maintained at a level near ten is limited to approximately 0.1 μs as a result of ionization instability.

[5]On the basis of this comparison it can also be concluded that the factors dominating ionization instability in rare-gas halide lasers are reasonably represented by the approximate expression for the instability growth rate given in (2).

IV. Summary and Discussion

The analysis and discussion of the preceding sections focuses attention on the relationship among the numerous processes contributing to the formation and loss of the KrF* molecule in an electron-beam controlled discharge. Therein it is shown that KrF* can be produced with an efficiency of 20 percent using this scalable excitation technique. In addition, krypton-monofluoride densities in excess of 10^{14} cm^{-3} are readily attained which, when combined with a stimulated emission cross section of about 2.4×10^{-16} cm^2, results in a gain coefficient of about 1 percent cm^{-1}. Thus, it can be concluded that KrF* kinetic processes are generally very favorable for efficient laser operation under conditions typical of near atmospheric pressure electron-beam controlled discharges.

The plasma required to achieve optimum KrF* laser excitation is characterized by a mean electron energy of several electron volts, a fractional ionization greater than 10^{-6}, and a fractional metastable concentration in excess of 10^{-5}. Section II shows that under these conditions electron-electron col-

lisions and electron collisions with excited atoms have a very important effect on plasma processes. Further, it is shown that numerous reactions, including rare-gas halide formation, result in dissociation of the fluorine fuel molecules. Since reactions between halogen molecules and both metastable atoms and electrons exert a controlling influence on the population of these species, dissociation of F_2 results in significant changes in plasma properties. Indeed, the results presented here show that as a result of F_2 dissociation, KrF* laser properties are continuously changing from the time of plasma initiation until termination due either to the onset of instability or to critical loss of F_2. For values of discharge: *e*-beam power enhancement greater than about three, results obtained to date have shown that plasma instability limits maximum laser pulse duration to a time less than 1 μs (Figs. 19-20). However, with E/n values corresponding to enhancement factors in the 2-3 range, laser pulses of about 1 μs have been achieved [1], with eventual loss of F_2 being the factor limiting pulse duration. This general behavior is typical of all electron-beam controlled rare-gas halide lasers [1], [35] and of the closely related mercury-halide [38] lasers as well.

Based on the good agreement between measured and predicted laser characteristics, it is reasonable to conclude that the dominant reactions influencing rare-gas halide formation and loss have been identified and that a satisfactory data base exists. However, operational experience with rare-gas halide lasers has, for the most part, been limited to single pulse experiments [1]. Practical implementation of this unusually promising class of high-power lasers requires dependable, repetitive pulse operation using a flowing, recirculating gas mixture. In addition, many applications will require electron-beam controlled discharge excitation under conditions such that the *e*-beam power is a relatively small fraction (<0.1) of the discharge power. Past experience with IR molecular lasers indicates that the major obstacles to achieving these objectives will be related to plasma chemical processes and discharge stability [39]-[41]. Solution of these formidable problems will require substantial additions to the existing body of knowledge pertaining to rare-gas halide kinetics. Aside from the primary reactions directly involved in rare-gas halide molecular processes, very little data exist for reactions between halogen molecules (and atoms) and discharge species. For example, there is little or no information pertaining to the reaction of either F atoms or F_2 with rare-gas excited states, electrons, or ions [42]. While reactions of this type may play only a secondary role in rare-gas monohalide molecule formation and loss as it occurs in a single pulse experiment, they are certain to exert an important influence on the chemistry of closed-cycle, repetitive pulse lasers.

Analysis of positive ion reactions in rare-gas halide plasmas is based almost entirely on the premise that rare-gas monomer and dimer ions are dominant. However, in addition to these ions, rare-gas trimer ions, heteronuclear rare-gas dimer ions, and rare-gas halide ions are likely to be present in significant concentrations ($\gtrsim$10 percent). It is known that relatively small concentrations of complex ions can significantly influence plasma properties [43] (especially stability [41]) because of their unusually large electron recombination coefficients [44]. In addition, positive ions play a unique role in rare-gas halide lasers as a consequence of their direct involvement in rare-gas halide formation [1], [5] and because they absorb radiation at the laser wavelength [32], [45]. For these reasons, improved knowledge of ion reactions at high pressure and low temperature is also of importance, especially under closed-cycle conditions for which the concentration of neutral species produced by plasma-chemical reactions is likely to become substantial.

Experimental verification [1] of the high energy conversion efficiency predicted for the KrF* laser represents a significant milestone in the development of a scalable, high power UV laser, and provides impressive evidence that conditions optimum for efficient laser excitation can be created in a high pressure, chemically active plasma. However, it has also been found that it is exceptionally difficult to *maintain* the desired plasma properties in a stable, long pulse ($\sim\mu$s) discharge because of significant changes in the gas mixture arising from the rare-gas halide formation process itself. As these systems are scaled for applications requiring high average power, difficulties arising from this circumstances will certainly become more pronounced. For this reason, it is clear that future efforts must be directed toward identification of the dominant ion and neutral chemical reactions occurring under the plasma conditions to be encountered with closed-cycle, respectively pulsed rare-gas halide lasers.

Acknowledgment

It is a pleasure to acknowledge the comments of R. T. Brown, which were particularly helpful in the preparation of this paper. Useful discussions with R. H. Bullis, H. H. Michels, L. A. Newman, and W. J. Wiegand are also appreciated.

References

[1] M. Rokni, J. A. Mangano, J. H. Jacob, and J. C. Hsia, "Rare gas fluoride lasers," *IEEE J. Quantum Electron.*, vol. QE-14, pp. 464-481, July 1978.
[2] J. J. Ewing, "Rare-gas halide lasers," *Phys. Today*, vol. 31, pp. 32-39, May 1978.
[3] J. E. Velazco and D. W. Setser, "Bound-free emission spectra of diatomic xenon halides," *J. Chem. Phys.*, vol. 62, pp. 1990-1991, Mar. 1, 1975.
[4] P. J. Hay and T. H. Dunning, Jr., "The electronic states of KrF," *J. Chem. Phys.*, vol. 66, pp. 1306-1316, Feb. 1977.
[5] M. Rokni, J. H. Jacob, and J. A. Mangano, "Dominant formation and quenching processes in *e*-beam pumped ArF* and KrF* lasers," *Phys. Rev. A*, vol. 16, pp. 2216-2224, Dec. 1977.
[6] J. H. Jacob and J. A. Mangano, "Modeling the KrF* laser discharge," *Appl. Phys. Lett.*, vol. 28, pp. 724-726, June 15, 1976.
[7] W. B. Lacina and D. B. Cohn, "Theoretical analysis of the electrically excited KrF* laser," *Appl. Phys. Lett.*, vol. 32, pp. 106-108, Jan. 15, 1978.
[8] A. J. DeMaria, "Review of high-power CO_2 lasers," in *Principles of Laser Plasmas*, G. Bekefi, Ed. New York: Wiley, 1976.
[9] J. D. Daugherty, "Electron-beam ionized lasers," in *Principles of Laser Plasmas*, G. Bekefi, Ed. New York: Wiley, 1976.
[10] W. L. Nighan, "Influence of molecular dissociation and degree of ionization on rare-gas halide laser properties," *Appl. Phys. Lett.*, vol. 32, pp. 424-426, Apr. 1, 1978.
[11] R. J. Hall, "Dissociative attachment and vibrational excitation of F_2 by slow electrons," *J. Chem. Phys.*, vol. 68, pp. 1803-1807, Feb. 15, 1978.
[12] W. L. Nighan, "Influence of electron-F_2 collisions in rare-gas halide laser discharges," *Appl. Phys. Lett.*, vol. 32, pp. 297-300, Mar. 1, 1978.
[13] P. J. Hay and D. C. Cartwright, "Rydberg, ionic and valence in-

teractions in the excited states of F_2," *Chem. Phys. Lett.*, vol. 41, pp. 80-82, July 1, 1976.
[14] M. V. Kurepa and D. S. Belic, "Dissociative attachment of electrons to chlorine molecules," *Chem. Phys. Lett.*, vol. 49, pp. 608-610, Aug. 1, 1977.
[15] W. C. Tam and S. F. Wong, "Dissociative attachment of halogen molecules by 0-8 eV electrons," *J. Chem. Phys.*, vol. 68, pp. 5626-5630, June 15, 1978.
[16] P. J. Chantry, "Attachment measurements in halogen bearing molecules," to be published.
[17] W. L. Borst, Excitation of metastable argon and helium atoms by electron impact," *Phys. Rev. A*, vol. 9, pp. 1195-1200, Mar. 1974.
[18] D. Rapp and P. Englander-Golden, "Total cross sections for ionization and attachment in gases by electron impact. I. Positive ionization," *J. Chem. Phys.*, vol. 43, pp. 1464-1479, Sept. 1, 1963.
[19] S. D. Rockwood, "Elastic and inelastic cross-sections for electron-Hg scattering from Hg transport data," *Phys. Rev. A.*, vol. 8, pp. 2348-2358, Nov. 1973.
[20] W. H. Long, Jr., "Electron kinetics in the KrF laser," *Appl. Phys. Lett.*, vol. 31, pp. 391-393, Sept. 15, 1977.
[21] H. A. Hyman, "Electron impact excitation of metastable argon and krypton," *Phys. Rev. A*, to be published.
[22] D. Ton-That and M. R. Flannery, "Cross sections for ionization of metastable rare-gas atoms (Ne^*, Ar^*, Kr^*, Xe^*) and of metastable N_2^*, CO^* molecules by electron impact," *Phys. Rev. A*, pp. 517-526, Feb. 1977.
[23] Cross sections for ionization of rare gas atoms from their p states were obtained using Gryzinski's formula (*Phys. Rev.*, vol. 138, pp. A336-A358, Apr. 19, 1963). As a check on the validity of this approximation for the conditions of interest, Gryzinski cross sections for ionization of rare-gas metastable states were generated and were found to be in good agreement with those of [22].
[24] W. L. Nighan, "Electron energy distributions and collision rates in electrically excited N_2, CO, and CO_2," *Phys. Rev. A*, vol. 2, pp. 1989-2000, Nov. 1970.
[25] J. E. Velazco, J. H. Kolts, and D. W. Setser, "Quenching rate constants for metastable argon, krypton, and xenon atoms by fluorine containing molecules and branching ratios for XeF^* and KrF^* formation," *J. Chem. Phys.*, vol. 65, pp. 3468-3480, Nov. 1, 1976.
[26] L. G. Piper and D. W. Setser, "Electronic energy transfer from metastable argon atoms to krypton atoms.", *J. Chem. Phys.*, vol. 63, pp. 5018-5028, Dec. 1, 1975.
[27] G. P. Quigley and W. M. Hughes, "The radiative lifetime and quenching of KrF," *Appl. Phys. Lett.*, vol. 32, pp. 627-629, May 15, 1978; also, J. G. Eden, R. W. Waynant, S. K. Searles, and R. Burnham, "New quenching rates applicable to the KrF lasers," *Appl. Phys. Lett.*, vol. 32, pp. 733-735, June 1, 1978.
[28] —, "Lifetime and quenching rate constants for Kr_2F^* and Kr^*," *Appl. Phys. Lett.*, vol. 32, pp. 649-651, May 15, 1978.
[29] P. J. Hay and T. H. Dunning, "The covalent and ionic states of the rare-gas monofluorides," *J. Chem. Phys.*, to be published.
[30] R. S. F. Chang and D. W. Setser, "Radiative lifetimes and two-body deactivation rate constants for $Ar(3p^5, 4p)$ and $Ar(3p^5, 4p')$ states," *J. Chem. Phys.*, to be published.
[31] R. T. Brown and W. L. Nighan, "Instability onset in electron-beam sustained KrF^* laser discharges," *Appl. Phys. Lett.*, vol. 32, pp. 730-732, June 1, 1978.
[32] A. M. Hawryluk, J. A. Mangano, and J. H. Jacob, "Gain and absorption measurements in a KrF^* laser," *Appl. Phys. Lett.*, vol. 31, pp. 164-166, Aug. 1, 1977.
[33] C. H. Fisher and R. E. Center, "Threshold power density measurements for electron-beam sustained discharge excitation of XeF^* and KrF^*, *Appl. Phys. Lett.*, vol. 31, pp. 106-108, July 15, 1977.
[34] J. A. Mangano, J. H. Jacob, and J. B. Dodge, "Electron-beam controlled discharge pumping of the XeF laser," *Appl. Phys. Lett.*, vol. 29, pp. 426-428, Oct. 1, 1976.
[35] L. F. Champagne and N. W. Harris, "Characteristics of the electron-beam controlled XeF laser," *Appl. Phys. Lett.*, to be published.
[36] J. D. Daugherty, J. A. Mangano, and J. H. Jacob," Attachment dominated electron-beam ionized discharges," *Appl. Phys. Lett.*, vol. 28, pp. 581-583, May 15, 1976.
[37] W. H. Long, Jr., "Discharge stability in *e*-beam sustained rare-gas halide lasers," to be published.
[38] J. H. Parks, "Laser action on the $B^2\Sigma^+_{1/2} \rightarrow X^2\Sigma^+_{1/2}$ band of HgCl at 5576 A°, *Appl. Phys. Lett.*, vol. 31, pp. 192-194, Aug. 1, 1977; also, W. T. Whitney, "Sustained discharge excitation of HgCl and HgBr $B^2\Sigma^+_{1/2} \rightarrow X^2\Sigma^+_{1/2}$ lasers," *Appl. Phys. Lett.*, vol. 32, pp. 239-241, Feb. 15, 1978.
[39] W. L. Nighan, "Stability of high-power molecular laser discharges," in *Principles of Laser Plasmas*, G. Bekefi, Ed. New York: Wiley, 1976.
[40] —, "Causes of thermal instability in externally sustained molecular discharges," *Phys. Rev. A*, vol. 15, pp. 1701-1720, Apr. 1970.
[41] —, "Influence of recombination and ion chemistry on the stability of externally sustained molecular discharges," *Phys. Rev. A*, vol. 16, pp. 1209-1223, Sept. 1977.
[42] E. W. McDaniel, M. R. Flannery, H. W. Ellis, F. L. Eisele, W. Pope, and T. G. Roberts, "Compilation of data relevant to rare gas-rare gas and rare gas-monohalide excimer lasers: Volumes 1 and 2," U.S. Army Missile Research and Development Command (DRDMI-TI), Rep. H-78-1, Dec. 1977.
[43] C. W. Werner, E. Zamir, and E. V. George, "Pressure dependence of the electron density in electron-beam-excited rare-gas plasmas," *Appl. Phys. Lett.*, vol. 29, pp. 236-239, Aug. 15, 1976.
[44] M. A. Biondi, "Recombination," in *Principles of Laser Plasmas*, G. Bekefi, Ed. New York: Wiley, 1976.
[45] W. R. Wadt, D. C. Cartwright, and J. S. Cohen, "Theoretical absorption spectra for Ne_2^+, Ar_2^+, Kr_2^+, and Xe_2^+ in the near ultraviolet," *Appl. Phys. Lett.*, vol. 31, pp. 672-674, Nov. 15, 1977.

SEPTEMBER 1976

DISTRIBUTION LIST FOR ONR PHYSICS PROGRAM OFFICE
UNCLASSIFIED CONTRACTS

Director — 3 copies
Defense Advanced Research Projects Agency
Attn: Technical Library
1400 Wilson Blvd.
Arlington, Virginia 22209

Office of Naval Research — 3 copies
Physics Program Office (Code 421)
800 North Quincy Street
Arlington, Virginia 22217

Office of Naval Research — 1 copy
Assistant Chief for Technology (Code 200)
800 North Quincy Street
Arlington, Virginia 22217

Naval Research Laboratory — 3 copies
Department of the Navy
Attn: Technical Library
Washington, D. C. 20375

Office of the Director of Defense — 3 copies
Research and Engineering
Information Office Library Branch
The Pentagon
Washington, D. C. 20301

U. S. Army Research Office — 2 copies
Box CM, Duke Station
Durham, North Carolina 27706

Defense Documentation Center — 12 copies
Cameron Station (TC)
Alexandria, Virginia 22314

Director, National Bureau of Standards — 1 copy
Attn: Technical Library
Washington, D. C. 20234

Commanding Officer — 3 copies
Office of Naval Research Branch Office
536 South Clark Street
Chicago, Illinois 60605

San Francisco Area Office — 3 copies
Office of Naval Research
760 Market Street, Room 447
San Francisco, California 94102

Office of Naval Research — 6 copies
Code 102 1P (ONR/L)
800 North Quincy Street
Arlington, Virginia 22217

Air Force Office of Scientific Research — 1 copy
Department of the Air Force
Washington, D. C. 22209

Commanding Officer — 3 copies
Office of Naval Research Branch Office
1030 East Green Street
Pasadena, California 91101

Commanding Officer — 3 copies
Office of Naval Research Branch Office
495 Summer Street
Boston, Massachusetts 02210

Director — 1 copy
U. S. Army Engineering Research
and Development Laboratories
Attn: Technical Documents Center
Fort Belvoir, Virginia 22060

ODDR&E Advisory Group on Electron Devices — 3 copies
201 Varick Street
New York, New York 10014

New York Area Office — 1 copy
Office of Naval Research
715 Broadway, 5th Floor
New York, New York 10003

Air Force Weapons Laboratory — 1 copy
Technical Library
Kirtland Air Force Base
Albuquerque, New Mexico 87117

Air Force Avionics Laboratory — 1 copy
Air Force Systems Command
Technical Library
Wright-Patterson Air Force Base
Dayton, Ohio 45433

Lawrence Livermore Laboratory — 1 copy
Attn: Dr. W. F. Krupke
University of California
P. O. Box 808
Livermore, California 94550

Harry Diamond Laboratories — 1 copy
Technical Library
Connecticut Ave. at Van Ness, N. W.
Washington, D. C. 20008

Naval Air Development Center — 1 copy
Attn: Technical Library
Johnsville
Warminster, Pennsylvania 18974

Naval Weapons Center — 1 copy
Technical Library (Code 753)
China Lake, California 93555

Naval Training Equipment Center — 1 copy
Technical Library
Orlando, Florida 32813

Naval Underwater Systems Center — 1 copy
Technical Library
New London, Connecticut 06320

Commandant of the Marine Corps — 1 copy
Scientific Advisor (Code RD-1)
Washington, D. C. 20380

Naval Ordnance Station — 1 copy
Technical Library
Indian Head, Maryland 20640

Naval Postgraduate School — 1 copy
Technical Library (Code 0212)
Monterey, California 93940

Naval Missile Center — 1 copy
Technical Library (Code 5632.2)
Point Mugu, California 93010

Naval Ordnance Station — 1 copy
Technical Library
Louisville, Kentucky 40214

Commanding Officer — 1 copy
Ocean Research & Development Activity
National Space Technology Laboratories
Bay St. Louis, Mississippi 39520

Naval Explosive Ordnance Disposal Facility — 1 copy
Technical Library
Indian Head, Maryland 20640

Naval Electronics Laboratory Center — 1 copy
Technical Library
San Diego, California 92152

Naval Undersea Center — 1 copy
Technical Library
San Diego, California 92132

Naval Surface Weapons Center — 1 copy
Technical Library
Dahlgren, Virginia 22448

Naval Ship Research and Development Center — 1 copy
Central Library (Code L42 and L43)
Bethesda, Maryland 20084

Naval Surface Weapons Center — 1 copy
Technical Library
Silver Spring, Maryland 20910

Naval Avionics Facility — 1 copy
Technical Library
Indianapolis, Indiana 46218